This is a preprint, the final version is subject to change, of the American Mineralogist (MSA)
Cite as Authors (Year) Title. American Mineralogist, in press.
(DOI will not work until issue is live.) DOI: http://dx.doi.org/10.2138/am-2015-5325

Hf and Nd isotope systematics of early Archean komatiites from surface sampling and ICDP drilling in the Barberton Greenstone Belt, South Africa

Janne Blichert-Toft[a,*], Nicholas T. Arndt[b], Allan Wilson[c], and Grace Coetzee[c]

[a]Laboratoire de Géologie de Lyon, Ecole Normale Supérieure de Lyon, Université Claude Bernard Lyon 1, and CNRS, 69007 Lyon, France

[b]ISTerre, Université Grenoble Alpes, 38041 Grenoble, France

[c]School of Geosciences, University of the Witwatersrand, Johannesburg, South Africa

*Corresponding author: Janne Blichert-Toft (jblicher@ens-lyon.fr; +33 4 72728488; +33 6 08134849)

Invited submission to *American Mineralogist's* Centennial Papers

Revised manuscript (**REVISION 1**) submitted May 13, 2015

ABSTRACT

To constrain the origin of komatiites from the Barberton Greenstone Belt, South Africa, we measured ^{147}Sm-^{143}Nd and ^{176}Lu-^{176}Hf compositions for 18 komatiites from core obtained during the International Continental Drilling Program in the Komati Formation of the Barberton Belt, as well as 33 komatiites from surface outcrops of the Komati, Hooggenoeg, and Weltevreden Formations, these latter for purposes of comparison between core and surface samples. Magmatic clinopyroxene from surface samples near the drill site was also analyzed. For the Lu-Hf isotope system, the Komati Formation core and surface samples including the clinopyroxene define a linear array whose slope corresponds to an age of 3426 ±

16 Ma (MSWD = 118; $\varepsilon_{Hf(T)}$ = +2.2), which is slightly younger than the accepted age of the rocks (3.48 Ga). The Sm-Nd isotope data for the same set of samples likewise fall along a linear array also yielding a younger age of 3339 ± 12 Ma (MSWD = 42; $\varepsilon_{Nd(T)}$ = +2.8). The high MSWD for both isotope systems indicate substantial scatter at variance with normal magmatic processes, likely implying element mobility disturbing even these relatively robust isotopic systems shortly after eruption of the lavas. The average initial ε_{Nd} and ε_{Hf} of the core samples at 3.48 Ga are +0.45 and +1.4, respectively, in overall accordance with the positive errorchron intercepts and a depleted mantle source at 3.5 Ga. In contrast, the clinopyroxene and their host rocks have strongly positive $\varepsilon_{Hf(T)}$ of about +5 and negative $\varepsilon_{Nd(T)}$ of about -2. Given the overall scatter of the whole-rock data, the most robust constraint on the composition of the komatiite source comes from the clinopyroxene. Their positive $\varepsilon_{Hf(T)}$ is in line with, though somewhat higher than other results from komatiites from the Komati Formation, but their negative $\varepsilon_{Nd(T)}$ is unexpected in that it indicates a source with long-term low Sm/Nd, which is at odds with its long-term high Lu/Hf. This signature is also found in the trace element compositions of some of the komatiites, such as moderately enriched LREE, negative Hf anomalies, and low Hf/Sm ratios. The origin of these features is uncertain but one possibility is that the discordance between the Hf and Nd isotope systems reflects the presence of deep-sea sediments in the source of some of the Barberton komatiites. The possible presence of a surface component in an ancient deep mantle source has wide-ranging implications for mantle-crust interaction and dynamics in the early Earth and for constraining a minimum age for the onset of plate tectonics.

Keywords: Komatiites, clinopyroxene, deep-sea sediment, chert, Barberton Greenstone Belt, Lu-Hf isotopes, Sm-Nd isotopes, International Continental Drilling Program, Invited Centennial article

INTRODUCTION

It is widely, if not universally, accepted that komatiite magmas result from melting in unusually hot parts of the mantle (e.g., Arndt et al. 2008; Herzberg 1992; Herzberg et al. 2010; Herzberg and O'Hara 1985; Walter 1998). The combination of high MgO contents and low concentrations of incompatible trace elements points to high degrees of partial melting, and geochemical evidence of garnet in the solid residue is consistent with melting at usually great depth (Green, 1974; 1981; Nesbitt et al. 1979; Ohtani et al. 1988; Sun and Nesbitt 1978). Most authors propose that the source was a mantle plume and that melting took place at depths of at least 200 km. Robin-Popieul et al. (2012) developed a model for the formation of komatiites from the type area in the Barberton Greenstone Belt of South Africa that has the Al-depleted, or Barberton-type, komatiite forming as batch melts at about 300 km depth and the Al-undepleted, or Munro-type, komatiite forming as advanced fractional melts at about 200 km depth. Schmeling and Arndt (in preparation) quantified the process taking into account the contrasting densities of melt and residual minerals and concluded that the melt segregated from the source in a series of high-volume pulses.

Radiogenic isotopes place constraints on the composition and history of the source and therefore allow insight into komatiite-forming processes and conditions of formation. No komatiites are pristine – all have undergone hydrothermal alteration at or near the seafloor, followed by metamorphism during accretion of the volcanic sequence to the continents and associated deformation. These processes could have affected their isotopic compositions to a degree that depends on the intensity of the alteration and the relative mobility of parent and daughter isotopes. Early attempts using the Rb-Sr isotope system produced no useful data from whole-rock samples but did give meaningful results from separated magmatic pyroxene (Machado et al. 1986).

The existing Nd and Hf isotope compositions of komatiites on a worldwide basis are summarized in Figure 1, including the data from this study. It is immediately apparent that the data scatter widely arising most likely from element mobility that disturbed even these relatively robust isotopic systems and hence for the most part do not represent primary mantle compositions. Although there is a general trend of increasing ε_{Nd} (Fig. 1a) and ε_{Hf} (Fig. 1b) with time, these trends are largely masked by the dispersion of the data. A more coherent trend is obtained when samples are carefully selected so as to include only those least altered, such as done by Puchtel et al. (2013), or by analysing separated magmatic pyroxene (J. Blichert-Toft, unpublished data not from the Barberton Greenstone Belt). Data selected in this way show an increase from values close to chondritic for the oldest samples to $\varepsilon_{Nd} \approx +10$ and $\varepsilon_{Hf} \approx +18$ for the youngest komatiites from Gorgona Island (not shown; Thompson et al. 2004).

Robin-Popieul et al. (2012) recognized three main types of komatiite among surface samples from the Barberton Greenstone Belt. These are (as summarized in Figures 2 and 3): (1) Al-depleted or classical Barberton-type komatiites which have relatively low Al_2O_3/TiO_2 ratios coupled with relative depletion of the heavy rare earth elements (HREE) (74% of sample suite; Figs. 2 and 3a); (2) samples with intermediate Al_2O_3/TiO_2 ratios and nearly flat REE patterns (18% of sample suite; Figs. 2 and 3b); (3) samples with high Al_2O_3/TiO_2 ratios and strongly sloping LREE-depleted patterns (8% of sample suite; Figs. 2 and 3c)(Wilson 2003). Robin-Popieul et al. (2012) explained these patterns in terms of contrasting melting mechanisms. The Al-depleted komatiites formed as batch melts deep in the mantle, whereas the Al-enriched types were the products of advanced fractional melting.

Most previously published Nd and Hf isotope data for komatiites from outcrops in the Barberton Greenstone Belt scatter widely. In the compilation reported in Figure 1, initial ε_{Nd}

values extend from about -3 to +5 (Fig. 1a) and initial ε_{Hf} values from about -3 to +10 (with two outliers from this study, BD2 and BD5, at ε_{Hf} of -13 and -15, respectively, falling off scale; Fig. 1b). Using samples selected on the basis of good preservation of primary magmatic mineralogical features, Puchtel et al. (2013) obtained $\varepsilon_{Nd(T)} = +0.46 \pm 0.10$ and $\varepsilon_{Hf(T)} = +1.9 \pm 0.3$ for the 3.48 Ga Komati Formation and $\varepsilon_{Nd(T)} = +0.50 \pm 0.11$ and $\varepsilon_{Hf(T)} = +4.7 \pm 0.8$ for the 3.27 Ga Weltevreden Formation. Combining these results with Os isotope data, Puchtel et al. (2014) developed a model that attributes these geochemical characteristics to melting of a depleted source produced by segregation of Mg- and Ca-perovskite in a ca. 4.5 Ga magma ocean.

In this paper we report ^{147}Sm-^{143}Nd and ^{176}Lu-^{176}Hf compositions for several suites of samples from the Barberton Greenstone Belt. These are (i) material from core drilled into the 3.48 Ga Komati Formation by the International Continental Drilling Program (ICDP) (Arndt et al. 2010); locality 1 in Figures 4 and 5), (ii) a suite of samples collected from outcrop of the Komati Formation at the drilling site, and (iii) surface samples from the Hooggenoeg and Weltevreden Formations. Clinopyroxene and amphibole separated from two of the surface samples from the Komati Formation (in the immediate vicinity of the ICDP drill holes) were also measured for their Nd and Hf isotope compositions. For the surface sample suites the major and trace element data are published in Robin-Popieul et al. (2012), while for the core samples the major and trace element data will be published by Wilson et al. (in preparation). The Hooggenoeg and Weltevreden Formations are younger than the Komati Formation, with ages of about 3.3 Ga (Byerly et al. 1996). The Hooggenoeg Formation samples were collected at locality 4 in Figure 4, in the southern portion of the Barberton Belt, about 8 km northeast of the ICDP drill site. The Weltevreden Formation komatiites were collected in the northern portion of the belt, at locality K in Figure 4. These samples are described by Connolly et al. (2011).

Petrographic and trace element analyses of the core samples have revealed the presence of a komatiite type that was previously unknown in the Barberton Greenstone Belt in which compositions are controlled by both olivine and orthopyroxene (Coetzee 2014). Here we further show that the Nd and Hf isotopic data provide evidence of an unusual source in the Archean mantle. Finally, it is the first time radiogenic isotope data are presented for the ICDP cores that sampled the komatiites from the Komati Formation.

SAMPLES

Descriptions of the geology of the Barberton Belt are provided by Lowe and Byerly (2007) and information about the ICDP drilling site is given by Dann (2000) and Robin-Popieul et al. (2012). The locations of 12 surface samples of komatiite and komatiitic basalt collected from the drill site in addition to 18 drill core samples are shown in the geological map of Figure 5 and described below.

Two cores were drilled at the Tjakastad site, as shown in Figures 4 and 5. The BARB1 core intersected a "tumulus" unit, which is an unusual thick, strongly internally differentiated flow produced by inflation by resurgence of new magma within the original flow (Dann and Grove 2007; Dann 2001). The tumulus unit was followed by a series of more typical sequences of thin differentiated komatiite flows and komatiitic basalts. The BARB2 core was sited about 100 m to the northwest and intersected a greater thickness of the overlying sequence of komatiites and komatiitic basalts. Detailed logs of the drill cores are available on the ICDP web site (www.peeringintobarberton.com) and the positions of the samples analyzed in this study are shown on simplified summary logs of the two cores in Figure 6. Because of the steeply dipping and folded strata in the area the cores were drilled up-section in the stratigraphy such that progressively younger layers were intersected with increasing depth in

the drill holes. The peak temperature of the metamorphism is poorly constrained but there is no evidence of metamorphic hornblende in any of the samples analyzed here. Amphibole is seen in thin sections of the samples from which the clinopyroxene analyzed in this study was extracted but from its brown color and anhedral, interstitial habit, it is evident that this amphibole is magmatic. The metamorphic assemblage is chlorite and serpentine with minor tremolite resulting from both early and late-stage hydrous alteration. Therefore, peak temperatures would have been upper greenschist facies at a maximum. Most of the alteration was due to reaction with seawater on the ocean floor followed by reaction with crustal fluids during accretion to the continent (Cloete 1999). Like most rocks in Archean greenstone belts, the samples are completely undeformed with relict textures (both olivine and interstitial clinopyroxene) wholly intact and unsheared with no sign of crystal deformation. No metasediments are found in the part of the Komati Formation where the BARB1 and BARB2 cores were drilled.

With the exception of minor amounts of unaltered chromite, no magmatic minerals were encountered in the core samples and hence rock names used in the following sections and listed in the isotope data table (Table 1) are derived from the whole-rock compositions, taken to be those of the volcanic rocks at the time of eruption.

Eight of the 18 drill core samples are from the tumulus unit with one of these being from the basal olivine orthocumulate, two being harristic olivine cumulates, three being olivine or pyroxene spinifex samples, and two being hyaloclastites. Eight other samples are from cumulates or spinifex units of thin, differentiated komatiite flows, one sample is the upper chill of a komatiite flow, and one sample is a komatiitic basalt. Neodymium and Hf isotopic compositions for these samples are listed in Table 1.

The degree of alteration of the Hooggenoeg Formation samples is similar to that of the

Komati Formation komatiites, but the Weltevreden Formation samples are better preserved. In sample WP109, for example, most of the olivine and all of the clinopyroxene are unaltered.

Neodymium and Hf isotopic data also are reported for 33 samples collected from surface outcrops in other parts of the Barberton Greenstone Belt. These include 12 samples of komatiite from other locations in the Komati Formation including four from the BARB2 drill site, three of komatitiic basalt from the Hooggenoeg Formation (3.47 Ga), and 15 of komatiite from the Weltevreden Formation (3.27 Ga). The locations and background petrological and geochemical (major and trace element abundances) data for these samples are reported by Robin-Popieul et al. (2012), while the Nd and Hf isotope compositions are listed in Table 1.

Only very sparse occurrence of unaltered minerals (and no unaltered olivine) were observed in the sequence intersected by the drill cores, but unaltered orthopyroxene and clinopyroxene, together with relict unaltered olivine, are present in surface samples from Grace's Flow, a thick differentiated komatiite flow located immediately above the base of the BARB2 core. Eight samples were collected from outcrops of this flow; six olivine cumulates (BD1, BD2, BD18, GC1, GC2, and GC3 of which GC3 was not analyzed here, only the clinopyroxene separated from it), a clinopyroxene cumulate (PXITE), and an olivine spinifex lava (BD4) (Table 1). Three clinopyroxene fractions (GC1 cpx1, GC2 cpx2, and GC3 cpx3; Table 1) were separated from three of the olivine cumulates (GC1, GC2, and GC3). Only an impure fraction of magmatic amphibole (GC3 amph; Table 1) from the olivine cumulate GC3 was obtained. Pyroxene in the pyroxene cumulate sample PXITE (Table 1) was altered to amphibole and other secondary minerals and hence was not separated for isotopic analysis. In contrast, the PXITE whole-rock was analyzed to help constrain potential effects of alteration on clinopyroxene isotope systematics.

U-Pb zircon dating of felsic volcanic rocks within the Theespruit Formation, which underlies

the Komati Formation, yields ages ranging from 3544 ± 3 to 3547 ± 3 Ma (Kröner et al. 1996), while a layer of dacitic tuff within the Komati Formation and stratigraphically higher than the BARB1 and BARB2 drill cores has a zircon U–Pb age of 3482 ± 5 Ma (Armstrong et al. 1990). On this basis it can be inferred that the age of the komatiites from the Komati Formation studied here is between 3.48 and 3.55 Ga. We chose 3.48 Ga for all epsilon calculations.

The age of the Hooggenoeg Formation is between that of the underlying Komati Formation (3482 ± 5 Ma) and that of a felsic tuff at the base of the overlying Kromberg Formation (3416 ± 5 Ma; (Byerly et al. 1996). The Weltevreden Formation has been dated at 3263 ± 12 Ma using the Re-Os chronometer (Puchtel et al. 2014). This is consistent with the observation that the Weltevreden Formation seems to be correlated with the Mendon Formation, which contains ash layers dated at 3298 ± 3 Ma (Byerly et al. 1996). In this study we have used, respectively, 3.47 Ga and 3.27 Ga for the epsilon calculations of samples from the Hooggenoeg and Weltevreden Formations.

ANALYTICAL TECHNIQUES

The 18 core samples were prepared as powders at the University of the Witwatersrand, Johannesburg. After initial cleaning of all surface alteration, whole-rock samples were jaw crushed and then milled using a high-purity C-steel swing mill pre-cleaned with quartz sand and subsequently conditioned with small sample aliquots prior to powdering the main sample mass. Splits from these homogenized powders were divided for distribution to members of the Barberton Drilling Project Consortium and were used for the isotope work of this study.

For the Nd and Hf isotopic analyses, all sample dissolution procedures, using steel-jacketed Parr bombs, and Lu-Hf and Sm-Nd chemical separation and isotopic analysis were carried out

at the Ecole Normale Supérieure in Lyon. After dissolution in Parr bombs, Sm, Nd, Lu, and Hf were separated from ca. 350-700 mg aliquots (depending on the degree of depletion of the respective samples) of whole-rock powder by ion-exchange column chromatography and measured for their isotopic compositions by MC-ICP-MS (Nu Plasma 500 HR) coupled with a desolvating nebulizer DSN-100 according to the procedures described by Blichert-Toft et al. (2002; 1997), Blichert-Toft (2001), and Blichert-Toft and Puchtel (2010). Samarium, Nd, Lu, and Hf concentrations were determined by isotope dilution using >98% pure mixed ^{149}Sm-^{150}Nd and ^{176}Lu-^{180}Hf spikes added to the samples prior to dissolution. The "Rennes" in-house Nd and JMC-475 Hf standards were analyzed systematically between every one or two samples to monitor machine performance and allow for standard bracketing of the unknown samples. The measured sample values were normalized to the accepted values of 0.511961 ± 0.000013 (corresponding to 0.511856 for La Jolla; Chauvel and Blichert-Toft 2001) for ^{143}Nd/^{144}Nd of the "Rennes" in-house Nd standard and 0.282163 ± 0.000009 (Blichert-Toft et al. 1997) for ^{176}Hf/^{177}Hf of the JMC-475 Hf standard using sample-standard bracketing. Mass bias were corrected relative to ^{146}Nd/^{144}Nd = 0.7219 and ^{179}Hf/^{177}Hf = 0.7325 using an exponential law. Total procedural blanks for Sm, Nd, Lu, and Hf were less than 20, 50, 20, and 20 pg, respectively. Isochron calculations (ages, initial isotopic compositions, and MSWDs) were done using the MatLab least-squares software by F. Albarède (version 7.0, 2014), which is an algorithm of least-squares straight lines with correlated errors and is an open source implementation of Minster et al. (1979) as discussed in Albarède (1995). The error on the age provided by this software is the propagated analytical uncertainties and the associated MSWD reflects the scatter of the samples about the alignment. If MSWD < 1.7, the alignment defines a statistically significant isochron, whereas if MSWD > 1.7, the alignment signifies an errorchon. Errors applied to the measured ^{147}Sm/^{144}Nd and ^{176}Lu/^{177}Hf ratios were ± 0.2%, while errors applied to the measured ^{143}Nd/^{144}Nd and ^{176}Hf/^{177}Hf ratios

were ± 0.00002 and ± 0.00001, respectively, which were the external reproducibilities of the present analytical sessions as determined by the repeated standard measurements. In the rare cases where the in-run error was larger than the external reproducibility (see Table 1 for the samples in question), the in-run error was used for the least-squares calculations. The decay constants used were 6.54×10^{-12} a^{-1} for ^{147}Sm (Lugmair and Marti 1978) and 1.867×10^{-11} a^{-1} for ^{176}Lu (Scherer et al. 2001; Söderlund et al. 2004). The Nd and Hf epsilon notations were calculated using the Sm-Nd and Lu-Hf CHUR values of, respectively, $^{147}Sm/^{144}Nd = 0.1967$ and $^{143}Nd/^{144}Nd = 0.512638$ (Wasserburg et al. 1981) and $^{176}Lu/^{177}Hf = 0.0332$ and $^{176}Hf/^{177}Hf = 0.282772$ (Blichert-Toft and Albarède 1997). The Nd and Hf isotope data are listed in Table 1.

Clinopyroxene was separated using a sieved 150–212 micron fraction with finer material removed in suspension using deionized water. The magnetic fraction, which included magnetite, olivine, and possibly chromite, was removed using a Frantz magnetic separator. Less dense minerals were removed using bromoform resulting in a pyroxene concentrate containing both clinopyroxene and orthopyroxene. Clinopyroxene was then concentrated magnetically to a purity of 98%. Orthopyroxene was also separated but only a very small amount which was insufficient for isotope analysis with the final fraction containing a high proportion of magmatic amphibole.

RESULTS

Petrological and petrographic features of the core flows

The stratigraphically lowest unit sampled by drilling is the tumulus, a unit that, according to Dann (2000; 2001), is distinguished from other komatiite flows by the following features: (1) at 30-80 m thick, it is thicker than most komatiite flows; (2) it has an unusual lens-like form;

(3) it is capped by a thick carapace of vesicular, chilled, or hyaloclastic-textured lava; (4) it has a thick lower olivine cumulate made up of unusually large, completely serpentinized olivine grains; (5) it is strongly differentiated from olivine adcumulate at the base to pyroxene spinifex-textured lava in the center.

Overlying the tumulus is a series of thin differentiated komatiite flows followed by massive and spinifex-textured komatiites and komatiitic basalts. The entire stratigraphic sequence is shown in logs on websites of the Barberton drilling project (peeringintobarberton.org) and reproduced in simplified form in Figure 6.

The textures and mineralogy of these komatiites are, with two exceptions, like those of other komatiites of the Barberton Greenstone Belt, as initially described by Viljoen and Viljoen (1969). The dominant mineral is olivine, in both cumulates and spinifex-textured lavas. Skeletal clinopyroxene, minor chromite, and altered glass are interstitial phases. No fresh minerals were present in the drill core of this section, but fresh pyroxene and, less commonly, fresh olivine are found in some surface samples. However, original textures remain perfectly preserved. Unusual features are the larger size of cumulus olivine in the tumulus unit (ca. 1 mm compared with ca. 0.5 mm in most komatiite flows), and the presence of two pyroxenes (orthopyroxene and clinopyroxene) in some sub-units. Orthopyroxene is particularly abundant in the sequence of flows that immediately overlie the tumulus (from 89 to 118 m in BARB1).

Geochemical characteristics of the core samples

In the following we briefly describe the geochemical characteristics of the tumulus unit (data from Coetzee 2014):

- The tumulus unit is strongly differentiated from olivine cumulates with MgO contents up to 44% to gabbro with an MgO content of 9.4%.

- Linear trends for immobile elements such as Ti, Al, Zr, Hf, and the REE correspond to olivine control lines. Samples with <15% MgO plot on a line consistent with pyroxene fractionation, whereas mobile elements such as Ca, Rb, Sr etc. scatter widely.
- The hyaloclastites have high MgO contents between 30 and 33%. On the premise that these samples represent quenched aphyric lava, their compositions are those of the liquid that fed the lava flow.
- Axis intercepts on Al_2O_3 or TiO_2 vs MgO diagrams correspond to olivine with the composition Fo92. Using the procedure described by Robin-Popieul et al. (2012), this olivine is in equilibrium with liquid with the composition of the flowtop hyaloclastites.

On the basis of these observations it is concluded that this flow resulted from the eruption of a highly magnesian komatiitic lava. As described by Dann (2000; 2001), influx of lava into the flow caused up-doming up the carapace of chilled hyaloclastite-textured lava to produce the lens-like structure of the tumulus. The lava in the flow interior then differentiated to produce highly evolved liquids that crystallized with pyroxene spinifex textured gabbroic assemblages where differentiation was advanced. The presence of vesicles, and perhaps the large grain size and complete serpentinization, indicate the presence of a small amount of water. Mantle-normalized trace element patterns (Fig. 3a) are similar to those of typical Barberton Al-depleted komatiites. It is noteworthy that they lack typical subduction signatures, such as negative Nb-Ta anomalies and enriched incompatible element contents. It may therefore be deduced that these rocks did not form in a subduction setting and that the water was probably introduced by assimilation of hydrous rock en route to the surface.

The sequence of komatiite flows immediately overlying the tumulus unit, from 91.8 to 118 m depth in the BARB1 core, shows geochemical evidence of orthopyroxene fractionation

(Coetzee 2014; Wilson et al., in preparation), which is corroborated by the unusual association of both cumulus olivine and orthopyroxene observed in thin section. From their Al_2O_3/TiO_2 ratios (Fig. 2) and their mantle-normalized trace element patterns (Fig. 3a), these komatiites can be classified as typical Al-depleted or Barberton type.

Sm-Nd and Lu-Hf isotopic data

The Sm-Nd and Lu-Hf isotopic data for the core samples and the surface samples overlying the drilling traces are listed in Table 1 and plotted in Figures 7 and 8. They show the following features. The Sm-Nd and Lu-Hf isotope data for the 18 core whole-rocks, three clinopyroxene separates, their host whole-rocks, the pyroxene cumulate, and, for the Sm-Nd system, also the impure amphibole fraction, plot on linear arrays whose slopes, if interpreted as isochrons (although MSWDs indicate they are errorchrons), give ages that are nearly within error (Lu-Hf; Fig. 7), or slightly lower (Sm-Nd; Fig. 8) than the accepted age of the rocks of 3.48 Ga adopted here. The Lu-Hf array gives an age T of 3440 ± 16 Ma (MSWD = 122; $(^{176}Hf/^{177}Hf)_T = 0.280628 \pm 0.000009$, corresponding to $\varepsilon_{Hf(T)} = +2.1 \pm 0.3$) and the Sm-Nd array an age of 3377 ± 13 Ma (MSWD = 34; $(^{143}Nd/^{144}Nd)_T = 0.508257 \pm 0.000019$, corresponding to $\varepsilon_{Nd(T)} = +1.9 \pm 0.4$), compared with the U-Pb zircon ages of 3.48 to 3.55 Ga. Excluding the three analyses of clinopyroxene, which control both the Sm-Nd and the Lu-Hf arrays, their host rocks, and the pyroxene cumulate such that the core samples are regressed alone results in a steeper slope for the Sm-Nd system corresponding to an age of 3677 ± 85 Ma (MSWD = 30; $(^{143}Nd/^{144}Nd)_T = 0.507889 \pm 0.000106$, translating into $\varepsilon_{Nd(T)} = -19 \pm 2$; Fig. 8) and a shallower slope for the Lu-Hf system corresponding to an age of 2914 ± 41 Ma (MSWD = 30; $(^{176}Hf/^{177}Hf)_T = 0.280875 \pm 0.000021$, translating into $\varepsilon_{Hf(T)} = -1.5 \pm 0.8$; Fig. 7). Regressing only the seven samples from Grace's Flow (GC1, GC2, PXITE, BD1, BD2, BD4, and BD18) with the clinopyroxene (and, for the Sm-Nd system, also the impure amphibole, which is an extreme outlier for the Lu-Hf system (Table 1) and therefore excluded

from the regression of the latter) yields a Lu-Hf age of 3466 ± 18 Ma (MSWD = 22 with BD2 excluded as an outlier, see Table 1; $(^{176}Hf/^{177}Hf)_T = 0.280680 \pm 0.000011$, corresponding to $\varepsilon_{Hf(T)} = +4.5 \pm 0.4$; Fig. 7) and a Sm-Nd age of 3314 ± 12 Ma (MSWD = 53; $(^{143}Nd/^{144}Nd)_T = 0.508370 \pm 0.000018$, corresponding to $\varepsilon_{Nd(T)} = +4.8 \pm 0.4$; Fig. 8). The Lu-Hf age becomes 3468 ± 18 Ma (MSWD = 20; $(^{176}Hf/^{177}Hf)_T = 0.280678 \pm 0.000011$, corresponding to $\varepsilon_{Hf(T)} = +4.5 \pm 0.4$) if BD4 is also excluded as it falls slightly above the alignment in Figure 7. Finally, regressing all the Komati Formation samples together (again excluding BD2 and the impure amphibole from the Lu-Hf regression) gives a Lu-Hf age of 3426 ± 16 Ma (MSWD = 118; $(^{176}Hf/^{177}Hf)_T = 0.280640 \pm 0.000009$, translating into $\varepsilon_{Hf(T)} = +2.2 \pm 0.3$; Fig. 7) and a Sm-Nd age of 3339 ± 12 Ma (MSWD = 42; $(^{143}Nd/^{144}Nd)_T = 0.508323 \pm 0.000016$, translating into $\varepsilon_{Nd(T)} = +2.8 \pm 0.4$; Fig. 8).

$\varepsilon_{Hf(T)}$ values of the individual core whole-rock samples, calculated assuming an age of 3480 Ma, show a large range from +3.9 to -3.2 (Table 1, which also lists uncertainties on individual epsilon values). The two extreme values are from the tumulus unit as sampled by the BARB1 core. The average $\varepsilon_{Hf(T)}$ is positive, at +1.4 ± 0.3. The individual initial Hf isotope compositions cannot be related to either rock type, degree of alteration, or major or trace element compositions. The three clinopyroxene fractions have significantly higher $\varepsilon_{Hf(T)}$ values at 3.48 Ga than those of the core samples ranging from +2.5 to +5.9. These values were reproduced for two of the clinopyroxene (the smaller size of the third clinopyroxene fraction allowed for only one analysis) (Table 1). The two whole-rocks yielding two of the clinopyroxene separates have similarly high $\varepsilon_{Hf(T)}$ of +4.7 and +5.4.

$\varepsilon_{Nd(T)}$ values of the individual core whole-rock samples, likewise calculated assuming an age of 3480 Ma, vary from +2.2 to -2.3 (Table 1, which also lists uncertainties on individual epsilon values). The flow from the stratigraphically lowest differentiated komatiite sequence

of the BARB1 core has extreme values, but the sample with the lowest $\varepsilon_{Hf(T)}$ (-3.2) has the highest $\varepsilon_{Nd(T)}$ (+2.2) (Table 1). The average $\varepsilon_{Nd(T)}$ is slightly positive, at +0.45 ± 0.3. As for the initial Hf isotope compositions, no systematic relationships are evident between the initial Nd isotope compositions and stratigraphic position, texture, or degree of alteration. Nor do major and trace element compositions correlate with Nd isotopes. Multiple samples from individual units, such as the tumulus (BARB1-10.18 to BARB1-89.23) and the differentiated Grace's Flow (GC1, GC2, PXITE, BD1, BD2, BD4, BD18) from the stratigraphically lowest komatiite package, show considerable ranges of initial isotopic compositions. The differences in Sm/Nd ratios of the different units do not correspond to different initial isotopic compositions. The two clinopyroxene fractions measured in duplicate, however, have more constant and significantly lower $\varepsilon_{Nd(T)}$ values ranging from -1.6 to -2.3 and their host rocks both have similarly negative $\varepsilon_{Nd(T)}$ of -1.9 (Table 1).

The pyroxene cumulate shows the same positive $\varepsilon_{Hf(T)}$ (+4.4) and negative $\varepsilon_{Nd(T)}$ (-0.3) as the relatively unaltered komatiites from which the clinopyroxene were separated (Table 1). The impure amphibole fraction has $\varepsilon_{Hf(T)}$ of +31 and $\varepsilon_{Nd(T)}$ of +0.1 indicating the presence of accessory phases affecting in particular the Lu-Hf isotope system (Table 1).

To decide which initial isotope ratios to adopt we considered the following: (1) The core-only regressions, which yield markedly too young (Lu-Hf) and too old (Sm-Nd) ages and, hence, erroneous y-axis intercepts (Figs. 7 and 8), were disregarded; (2) we took into account only Grace's Flow and "all samples" regressions (Figs. 7 and 8); (3) despite the overall scatter about the errorchrons, the Lu-Hf errorchron seems to preserve nearly the correct age. On this basis we concluded that the errorchron initials provide a better estimate of the true initials than individual samples or averages of them. Nevertheless, the errorchron initials (at the age of the errorchrons) are similar to those of most of the individual samples at 3.48 Ga: almost

all show positive ε_{Hf} and, except for Grace's Flow's whole-rocks and clinopyroxene, positive ε_{Nd} (Figs. 7 and 8) consistent with depleted mantle evolution at 3.5 Ga.

As seen in Table 1, the surface samples display considerably more scatter, with some samples departing to extreme positive or negative values. However, when the most extreme outliers are excluded, the average $\varepsilon_{Nd(T)}$ and $\varepsilon_{Hf(T)}$ values are broadly similar to those obtained from the core samples. Taken separately, each of the Komati, Hooggenoeg, and Weltevreden sample suites shows a large range of calculated initial isotopic values. In each suite, one or more samples give extremely high or low values, particularly for the Lu-Hf isotope system, but less so for the Sm-Nd isotope system. Excluding the outliers (four in total), the mean $\varepsilon_{Nd(T)}$ and $\varepsilon_{Hf(T)}$ values are as follows: the Komati Formation, $\varepsilon_{Nd(T)}$ = -0.5 to +4.4 (one outlier, BD20, excluded), $\varepsilon_{Hf(T)}$ = +0.4 to +10.1 (two outliers, BD2 and BD5, excluded); the Hooggenoeg Formation, $\varepsilon_{Nd(T)}$ = +0.1 to +0.4, $\varepsilon_{Hf(T)}$ = +0.7 to +3.4 (the Lu-Hf measurement failed for HOG1); the Weltevreden Formation, $\varepsilon_{Nd(T)}$ = +0.5 to +2.2, $\varepsilon_{Hf(T)}$ = +3.9 to +13.4 (one outlier, MC6-4, excluded) (see Table 1 for uncertainties on the individual epsilon values). Again, these initial values are consistent with depleted mantle evolution in the early Archean. There are no systematic differences between the isotopic compositions of the three different groups of komatiite. Within the relatively large variability of the data, the $\varepsilon_{Hf(T)}$ values tend to become more positive with decreasing age, while the $\varepsilon_{Nd(T)}$ values remain essentially constant.

DISCUSSION

Although the ranges of parent-daughter isotope ratios for the drill core samples are not very large (hence the relatively large uncertainties on the ages obtained), these ranges are far

greater than can be expected from normal magmatic processes. In most of the flow units encountered in the core and at the drill site, olivine is the sole major fractionating phase and this phase does not fractionate Sm from Nd, nor Lu from Hf. The samples from the sequence between 91.8 and 118 m in the BARB1 core crystallized orthopyroxene in addition to olivine, but this phase also does not change either Sm/Nd or Lu/Hf. The fact that large variations in these isotope ratios are observed in single units (e.g., the tumulus and Grace's Flow) rules out the possibility that they resulted from different parental magma compositions. Although not impossible, it is mechanistically unlikely that magmas from different sources or different magma-crust interaction histories fed into the same flow system. As has been recognized in numerous other studies (e.g., Claoué-Long et al. 1984; Dupré et al. 1984), the processes that most likely caused these changes were secondary, such as hydrothermal alteration or metamorphism. The coincidence between the ages calculated for the Komati samples and the accepted eruption age, especially how remarkably within error of the assumed true age the Lu-Hf age is (Fig. 7), indicates that these secondary processes operated synchronously with, or very soon after, emplacement of the flows and may have been related to early seafloor alteration of the flows (Hoffmann and Bohlar 2007; Hoffmann and Wilson 2007). The relatively younger Sm-Nd errorchron (Fig. 8) may, however, rather reflect metamorphism occurring 10's or 100's of million years after komatiite emplacement, in which case this event did not affect the Lu-Hf isotope system to the same extent it impacted the Sm-Nd isotope system.

Given the scatter of the whole-rock data, and the fact that secondary processes influenced these systems, the best constraint on the composition of the source of these komatiites should come from the clinopyroxene separates. As shown in Table 1 for the Lu-Hf isotope system, the clinopyroxene have $\varepsilon_{Hf(T)}$ values that are higher than, though still within the range of, the whole-rock data from both this study and that of Puchtel et al. (2013). For the Sm-Nd isotope

system, however, the $\varepsilon_{Nd(T)}$ values of the clinopyroxene separates are negative (Table 1) and far lower than those of the whole-rocks for all studies conducted so far.

Figures 7 and 8 show Lu-Hf and Sm-Nd isochrons for the clinopyroxenes and samples of olivine spinifex, olivine cumulate, and pyroxene cumulate from the same flow. These isochrons give ages that are lower than the probable eruption age (3466 ± 18 Ma with MSWD = 22 for Lu-Hf and 3314 ± 12 with MSWD = 53 for Sm-Nd). However, given the large statistical uncertainties, the difference is probably not significant. Textures of these pyroxenes (Fig. 9) indicate they are primary magmatic and crystallized as an interstitial phase to the cumulus olivine, now partially to completely serpentinized. On this basis, the possibility that the pyroxenes are secondary or that later metamorphism reset their isotopic systems is rejected. We recognize that the mineral separates may contain small amounts of other phases (possibly highly fractionated components) due to the fine grain size. Indeed, the impure separate made to try to isolate magmatic amphibole has a highly anomalous composition (Table 1) and probably contains minor phases (monazite, zircon, baddelleyite, apatite) that fractionated the isotope systems, especially that of Lu-Hf. However, the consistent values of the clinopyroxenes for both isotope systems indicate that they are those of the original magmas. The presence of small amounts of secondary minerals may account for at least part of the variations in Sm/Nd and Lu/Hf of the clinopyroxene separates but it is difficult to suggest a phase which, in minor amounts, could drastically decrease the $\varepsilon_{Nd(T)}$ value while at the same time increase $\varepsilon_{Hf(T)}$ relative to the typical komatiite whole-rock values. The samples of olivine cumulate from which the three clinopyroxene were separated have a similar isotopic composition to the clinopyroxene separates (highly positive $\varepsilon_{Hf(T)}$ and negative $\varepsilon_{Nd(T)}$; Table 1). In addition, the whole-rock sample of pyroxene cumulate (PXITE), which contains about 70% cumulus clinopyroxene, now completely altered to secondary amphibole, has a

similar $\varepsilon_{Hf(T)}$ of +4.4, though an intermediate $\varepsilon_{(NdT)}$ of -0.3 (Table 1), which nevertheless is still significantly lower than that of the average whole-rock komatiites.

This decoupling of the two isotopic systems is difficult to explain. Normally, the two parent-daughter systems Sm-Nd and Lu-Hf fractionate in the same manner, and consequently the isotopic compositions should correlate positively. This is indeed the case in most suites of samples from both mantle and crustal sources (e.g., Vervoort and Blichert-Toft 1999; Vervoort et al. 1999), including the samples of Barberton komatiites analyzed earlier by us (Blichert-Toft and Arndt 1999; Blichert-Toft et al. 2004) and by Puchtel et al. (2013). In these data sets the whole-rocks have positive $\varepsilon_{Hf(T)}$ and $\varepsilon_{Nd(T)}$, values similar to the mean $\varepsilon_{Hf(T)}$ and $\varepsilon_{Nd(T)}$ values of the whole-rock core and surface samples of this study. Contrary to these expected results are the two clinopyroxenes of this study and their host rocks with their strongly positive $\varepsilon_{Hf(T)}$ and distinctly negative $\varepsilon_{Nd(T)}$.

This distinctive isotopic fingerprint indicates that the present komatiites were derived from a source with low time-integrated Sm/Nd and high time-integrated Lu/Hf. A trace element pattern consistent with these observations is illustrated schematically in Figure 10. The actual trace element patterns of the whole-rock samples from the differentiated komatiite flows, including the sample that yielded the clinopyroxenes measured here, have patterns that support this suggestion (Fig. 3a; trace element data from Coetzee 2014; Robin-Popieul et al. 2012; Wilson et al., in preparation).

One way of explaining the unusual clinopyroxene signature is the presence of a phase, or possibly several phases, that fractionate the two isotopic systems in opposite senses. In the upper mantle the phases that can change the parent-daughter ratios are clinopyroxene, or more effectively, garnet, but both these phases would act in the same sense for the two isotope systems. In all accepted data sets (e.g., Green 1994 and the GERM database

http://earthref.org/GERM/) the clinopyroxene and garnet partition coefficients for Sm is greater than those for Nd, and those for Lu greater than those for Hf. As a consequence, a clinopyroxene or garnet cumulate would evolve over time to positive values of both ε_{Nd} and ε_{Hf}, and the residual liquid would evolve to negative values. The same applies to common phases in the lower mantle. Ca-perovskite strongly fractionates both systems, but again in the same sense (Corgne and Wood 2005), while Mg-perovskite has little effect on these ratios (Corgne et al. 2005). Only fractionation of magnesiowüstite could produce the correct sense of change for both systems because Hf (but not the REE elements) is compatible with this phase (Hauri et al. 1996). The systematics are shown schematically in Figure 11. This explanation seems unlikely, however, simply because it would require that the proportion of magnesiowüstite in the residue be significantly higher than that of Ca- or Mg-perovskite, which is contrary to normal estimates of lower mantle compositions (Irifune and Tsuchiya 2007).

Another possibility is that the komatiite source contained a fraction of fine-grained sediment, which, owing to its paucity in zircons, would have a high Lu/Hf ratio and a relatively low Sm/Nd ratio. As argued by Patchett et al. (1984), Vervoort et al. (1999), and Garçon et al. (2013), the Lu-Hf and Sm-Nd isotope systems are decoupled in clastic sediments because zircon, which preferentially extracts Hf, is deposited in fluvial or coastal settings, while finer-grained sediment, depleted of zircon and therefore characterized by a Hf deficit and high Lu/Hf, is deposited in deeper waters. In the early Archean, because of the unusual composition of seawater and the absence of organisms with calcareous shells, the normal sediment on the oceanic floor was chert. Chemical analyses by Ledevin (2013) of Barberton cherts show that this type of sediment has particularly high Lu/Hf but moderate Sm/Nd, and isotopic analyses by Garçon et al. (2015) demonstrate that this material, as would be expected, evolves with time to produce high $\varepsilon_{Hf(T)}$ and low $\varepsilon_{Nd(T)}$.

This raises the possibility that the unusual composition of the clinopyroxene in Grace's Flow resulted from the incorporation of old chert into the komatiite, either via contamination of the komatiite magma during its passage to the surface or as a component in the source. We tested this idea by modeling both processes. The parameters used in the modeling are given in Table 2. The isotopic composition corresponds to a chert that is about 200 My older than the komatiite, the absolute maximum plausible age in the Barberton context.

Modeling of assimilation of chert into komatiite magma is straightforward because the Nd and Hf contents of chert and komatiite are similar. The result is clear: to produce the isotopic composition of Grace's Flow clinopyroxene requires a very large amount of contamination, 60%, and the assimilation of this much chert produces a contaminated magma containing 78% SiO_2, i.e. granite, not komatiite. An assimilation and fractional crystallization (AFC) process was not considered in this simple mixing scenario because the target isotopic composition would not be reached before complete solidification of the magma. This result clearly indicates that the unusual composition of Grace's Flow clinopyroxene cannot be the result of contamination during ascent of the komatiite magma.

If the chert were present in the source, the situation is more promising, for two reasons: first, the Nd and Hf concentration in the source are far lower, which means that less chert is required to change the isotopic composition of the mixture; second, the composition of the melt of a contaminated source is not directly related to the SiO_2 content. Table 2 shows that only about 10% chert is required and this amount of contamination produces a source containing about 50% SiO_2. If this source melted at high enough pressure, it could produce magma with a komatiitic composition.

Hence, addition to the komatiite source of ancient (early Archean) chert would be capable of increasing its Lu/Hf ratio while leaving the Sm/Nd ratio unchanged. Over time this material

would acquire an unusually positive ε_{Hf} for a given ε_{Nd} (Fig. 12). Therefore, as modeled above, if such material were recycled into the mantle and entrained in the source of the komatiites, this could explain both the trace element patterns and the Nd and Hf isotope systematics observed here. We do not exclude or find it unlikely that the samples of the present study showing initial ε_{Nd} and ε_{Hf} values similar to the komatiites analyzed by Puchtel et al. (2013) underwent the same magma ocean processes as proposed by these authors, but if so, this record has been overprinted in Grace's Flow with the distinct signature of sediments akin to the Barberton cherts.

Additional evidence in favor of fine-grained sediment in the source of the Komati Formation komatiites comes from the Hf/Sm ratio, which is well known to be nearly constant and close to chondritic (0.74 ± 0.03; Bouvier et al. 2008) in the vast majority of terrestrial magmatic rocks and therefore seems to be largely unaffected by later magmatic processes (Blichert-Toft and Albarède 1999). In Table 1, we report the calculated Hf/Sm ratios of the komatiites analyzed in this study, and in Figure 13 we show the data in the form of a frequency histogram including the Komati and Weltevreden Formation data from Puchtel et al. (2013). Using the Hf and Sm concentrations determined for all the samples by isotope dilution (Table 1 and (Puchtel et al. 2013) we find that the average Hf/Sm of the core komatiites is 0.58 (Fig. 13), while the surface samples from the Komati Formation (Grace's Flow and other outcrops) have average Hf/Sm of 0.64 (Fig. 13). The clinopyroxene separated from the whole-rocks from Grace's Flow have average Hf/Sm of 0.65 (Fig. 13). These values are all significantly lower than the CHUR value. In comparison, the komatiites from the Hooggenoeg and Weltevreden Formations have average Hf/Sm of 0.71 and 0.76, respectively (Fig. 13), identical within error to the CHUR value. The samples from the Komati Formation analyzed by Puchtel et al. (2013) also have low Hf/Sm averaging 0.60, while the samples from the Weltevreden Formation, likewise analyzed by Puchtel et al. (2013), have Hf/Sm ratios similar

to those of the Weltevreden Formation samples of the present study, averaging 0.74 (Fig. 13). The Hf/Sm data hence provide strong evidence for a Hf deficit in the source of the Komati Formation komatiites, which is consistent with the trace element patterns in Fig. 3a and the incongruous Nd and Hf isotope systematics of the clinopyroxene and their host rocks. This scenario resembles that observed for Hawaii, where combined Hf, Nd, and Pb isotope systematics indicate the presence of deep-sea sediments in the source of Hawaiian lavas (Blichert-Toft et al. 1999). The presence in the early Archean of crustally derived material in a deep mantle source, such as that inferred for the Barberton komatiites, potentially has wide implications for the understanding of plate tectonics and crust-mantle interaction in the early Earth.

IMPLICATIONS

The main message to emerge from this study is the difficulty in obtaining reliable and useful results from the analysis of old, variably altered volcanic rocks. Careful selection of the best-preserved samples in various parts of the Barberton greenstone belt can be successful, as demonstrated by Puchtel et al. (2013) for the Komati type locality. However, when a study focuses on a restricted region, as was the case in this study where the sampling was limited to the sequences intersected by the drill core, the choice of samples is limited, with potential detrimental consequences for the quality of the final results. A possible means of avoiding the effects of alteration on whole-rock samples is to separate relict magmatic minerals such as clinopyroxene. The analysis of clinopyroxene in this study provided evidence of a component of unusual composition in the source of the Barberton komatiites. The possible presence in the early Archean of crustally derived material in a deep mantle source potentially has wide implications for the understanding of plate tectonics and crust-mantle interaction in the early

Earth. The isotopic signature that we here attribute to fine-grained sediment is present only in a single flow and it is possible that the magma in this unit sampled a minor and unusual component in the mantle source. However, if this signature is more widely distributed, as is suggested by the corresponding trace element patterns and Hf/Sm ratios of some of the other flows also analyzed in this study, then this may indicate that sediment recycling in the early Archean was a more common phenomenon.

CONCLUSIONS

To constrain the nature and history of the early Archean Barberton mantle source, we measured Sm-Nd and Lu-Hf isotope compositions for a large number of komatiites from the Barberton Greenstone Belt, including samples from ICDP drill cores, and obtained what at first appeared to be puzzling results. The data define linear arrays whose slopes suggest an age of about 3.47 Ga for the Lu-Hf isotope system and 3.34 Ga for the Sm-Nd isotope system regardless of the samples regressed. While the former is close to the accepted emplacement age of the rocks of 3.48 Ga, the latter is too young. Average $\varepsilon_{Nd(T)}$ and $\varepsilon_{Hf(T)}$ at 3.48 Ga for the core whole-rocks are +0.5 and +1.4, respectively, while the clinopyroxene fractions from a surface sample of komatiite have $\varepsilon_{Nd(T)}$ = -2.3 to +2.1 and $\varepsilon_{Hf(T)}$ = +2.5 to +5.9, an incongruous signature also observed in their host rocks but not in the core samples. The results from the core whole-rocks are broadly in line with those obtained in previous studies of Barberton komatiites, while the distinctly negative $\varepsilon_{Nd(T)}$ accompanied by strongly positive $\varepsilon_{Hf(T)}$ of the clinopyroxene and their host rocks is unusual and difficult to explain. The clinopyroxenes are well preserved and retain magmatic texture and composition. Given that the isochron ages range from close to the accepted value (3.47 Ga for the Lu-Hf system) to distinctly younger (3.34 Ga for the Sm-Nd system), some disturbance from secondary processes of the isotope systems in these minerals cannot be ruled out. The near-coincidence

between the isochron ages and the accepted eruption age indicates that these secondary processes operated contemporaneously with, or very soon after emplacement of the flows, most likely by sea-water interaction with the hot lavas. A possible explanation for the peculiar source characteristics (time-integrated low Sm/Nd and high Lu/Hf) of the komatiite flow that yielded the clinopyroxene is that the source contained a component of fine-grained sediment (chert), an observation supported by trace element systematics and unusually low Hf/Sm ratios. The identification of what may be deep-sea sediment, a surface component, recycled into the deep mantle source of ancient komatiites has direct implications for crust-mantle dynamics and the timing of onset of plate tectonics in the early Earth.

ACKNOWLEDGMENTS

JBT and NTA thank the French Agence Nationale de la Recherche for financial support of this project through the grant ANR-10-BLANC-0603 M&Ms – Mantle Melting – Measurements, Models, Mechanisms, while AHW and GC thank the National Research Foundation (South Africa) for their financial aid. We further thank Philippe Telouk for assistance with the Nu Plasma MC-ICP-MS at ENS Lyon, Jan Wijbrans for providing the GC3 cpx3 and amphibole separates, Francis Albarède for discussion and making available his MatLab least-squares software, and Bill White and Igor Puchtel for constructive reviews.

REFERENCES CITED

Albarède, F. (1995) Introduction to Geochemical Modeling. Cambridge University Press.
Armstrong, R.A., Compston, W., De Wit, M.J., and Williams, I.S. (1990) The stratigraphy of the 3.5-3.2 Ga Barberton Greenstone Belt revisited: a single zircon ion microprobe study. Earth and Planetary Science Letters, 101, 90-106.
Arndt, N.T., Barnes, S.J., and Lesher, C.M. (2008) Komatiite. Cambridge University Press.
Arndt, N.T., Bruzak, G., and Reischmann, T. (2001) The oldest continental and oceanic plateaus: geochemistry of basalts and komatiites of the Pilbara Craton, Australia, in:

Ernst, R.E., Buchan, K.L. (Eds.), Mantle Plumes: their identification through time. Geological Society of America, Special Paper, Boulder, pp. 359-388.

Arndt, N.T., Kerr, A.C., and Tarney, J. (1997) Dynamic melting in plume heads: the formation of Gorgona komatiites and basalts. Earth and Planetary Science Letters, 146, 289-301.

Arndt, N.T., Wilson, A., Hofmann, A., Mason, P., Bau, M., Byerly, G., and Chunnett, G. (2010) Scientific drilling in the Barberton Greenstone Belt. Geobulletin, 53, 17-18.

Barrie, C.T., and Shirey, S.B. (1991) Nd-and Sr-isotope systematics for the Kamiskotia-Montcalm area: implications for the formation of late Archean crust in the western Abitibi Subprovince, Canada. Canadian Journal of Earth Sciences, 28, 58-76.

Blichert-Toft, J. (2001) On the Lu-Hf isotope geochemistry of silicate rocks. Geostandards Newsletter, 25, 41-56.

Blichert-Toft, J., and Albarède, F. (1997) The Lu-Hf isotope geochemistry of chondrites and the evolution of the mantle-crust system. Earth and Planetary Science Letters, 148, 243-258.

Blichert-Toft, J., and Albarède, F. (1999) Hf isotopic compositions of the Hawaii Scientific Drilling Project core and the source mineralogy of Hawaiian basalts. Geophysical Research Letters, 26, 935-938.

Blichert-Toft, J., and Arndt, N.T. (1999) Hf isotope compositions of komatiites. Earth and Planetary Science Letters, 171, 439-451.

Blichert-Toft, J., Arndt, N.T., and Gruau, G. (2004) Hf isotopic measurements on Barberton komatiites: effects of incomplete sample dissolution and importance for primary and secondary magmatic signatures. Chemical Geology, 207, 261-275.

Blichert-Toft, J., Boyet, M., Télouk, P., and Albarède, F. (2002) ^{147}Sm-^{143}Nd and ^{176}Lu-^{176}Hf in eucrites and the differentiation of the HED parent body. Earth and Planetary Science Letters, 204, 167-181.

Blichert-Toft, J., Chauvel, C., and Albarède, F. (1997) Separation of Hf and Lu for high-precision isotope analysis of rock samples by magnetic sector-multiple collector ICP-MS. Contributions to Mineralogy and Petrology, 127, 248-260.

Blichert-Toft, J., Frey, F.A., and Albarède, F. (1999) Hf isotope evidence for pelagic sediments in the source of Hawaiian basalts. Science, 285, 879-882.

Blichert-Toft, J., and Puchtel, I.S. (2010) Depleted mantle sources through time: Evidence from Lu-Hf and Sm-Nd isotope systematics of Archean komatiites. Earth and Planetary Science Letters, 297, 598-606.

Bouvier, A., Vervoort, J.D., and Patchett, P.J. (2008) The Lu-Hf and Sm-Nd isotopic composition of CHUR: constraints from unequilibrated chondrites and implications for the bulk composition of terrestrial planets. Earth and Planetary Science Letters, 273, 48-57.

Byerly, G.R., Kröner, A., Lowe, D.R., Todt, W., and Walsh, M.M. (1996) Prolonged magmatism and time constraints for sediment deposition in the early Archean Barberton greenstone belt: evidence from the Upper Onverwacht and Fig Tree groups. Precambrian Research, 78, 125-138.

Chauvel, C., Arndt, N.T., Kielinzcuk, S., and Thom, A. (1987) Formation of Canadian 1.9 Ga old continental crust: (1) Nd isotopic data. Canadian Journal of Earth Sciences, 24, 396-406.

Chauvel, C., and Blichert-Toft, J. (2001) A hafnium isotope and trace element perspective on melting of the depleted mantle. Earth and Planetary Science Letters, 190, 137-151.

Chauvel, C., Dupré, B., and Arndt, N.T. (1993) Pb and Nd isotopic correlation in Belingwe komatiites and basalts, in: Bickle, M.J., Nisbet, E.G. (Eds.), The geology of the Belingwe Greenstone Belt, Zimbabwe. Balkema, Rotterdam, pp. 167-174.

Chavagnac, V. (2004) A geochemical and Nd isotopic study of Barberton komatiites (South Africa): implication for the Archean mantle. Lithos, 75, 253-281.

Claoué-Long, J.C., Thirlwall, M.F., and Nesbitt, R.W. (1984) Revised Sm-Nd systematics of Kambalda greenstones, Western Australia. Nature, 307, 697-701.

Cloete, M. (1999) Aspects of volcanism and metamorphism of the Onverwacht Group lavas in the southwestern portion of the Barberton Greenstone Belt, Geological Survey of South Africa, pp. 229.

Coetzee, G. (2014) Petrology and geochemistry of the Tjakastad (Barberton) ICDP cores. University of the Witwatersrand, pp. 190.

Connolly, B.D., Puchtel, I.S., Walker, R.J., Arevalo, R., Piccoli, P.M., Byerly, G.R., Robin, C., and Arndt, N. (2011) Highly siderophile element systematics of the 3.3 Ga Weltevreden komatiites, South Africa. Earth and Planetary Science Letters, 311, 253-263.

Corgne, A., Liebske, C., Wood, B.J., Rubie, D.C., and Frost, D.J. (2005) Silicate perovskite-melt partitioning of trace elements and geochemical signature of a deep perovskitic reservoir. Geochimica et Cosmochimica Acta, 69, 485-496.

Corgne, A., and Wood, B. (2005) Trace element partitioning and substitution mechanisms in calcium perovskites. Contributions to Mineralogy and Petrology, 149, 85-97.

Dann, J., and Grove, T.L. (2007) Volcanology of the Barberton Greenstone Belt, South Africa: inflation and evolution of flow fields, in: Van Kranendonk, M.J., Smithies, R.H., Bennett, V.C. (Eds.), Earth's Oldest Rocks: Developments in Precambrian Geology. Elsevier, Amsterdam, pp. 527-570.

Dann, J.C. (2000) The Komati Formation, Barberton Greenstone Belt, South Africa, part I: new map and magmatic architecture. South African Journal of Earth Sciences, 6, 681-730.

Dann, J.C. (2001) Vesicular komatiites, 3.5-Ga Komati Formation, Barberton Greenstone Belt, South Africa: inflation of submarine lavas and origin of spinifex zones. Bulletin of Volcanology, 63, 462-481.

Dupré, B., Chauvel, C., and Arndt, N.T. (1984) Pb and Nd isotopic study of two Archean komatiitic flows from Alexo, Ontario. Geochimica et Cosmochimica Acta, 48, 1965-1972.

Garçon, M., Carlson, R.W., Shirey, S.B., Arndt, N.T., and Horan, M. (2015) Erosion of Archean continents: the Nd-Hf isotopic record of Barberton sedimentary rocks. 25th Annual V.M. Goldschmidt Conference, Prague.

Garçon, M., Chauvel, C., France-Lanord, C., Huyghe, P., and Lavé, J. (2013) Continental sedimentary processes decouple Nd and Hf isotopes. Geochimica et Cosmochimica Acta, 121, 177-195.

Green, D.H. (1974) Genesis of Archaean peridotitic magmas and constraints on Archaean geothermal gradients and tectonics. Geology, 3, 15-18.

Green, D.H. (1981) Petrogenesis of Archaean ultramafic magmas and implications for Archaean tectonics, in: Kröner, A. (Ed.), Precambrian Plate Tectonics. Elsevier, Amsterdam, pp. 469-490.

Green, T.H. (1994) Experimental studies of trace-element partitioning applicable to igneous petrogenesis - Sedona 16 years later. Chemical Geology, 117, 1-36.

Hanski, E., Huhma, H., Rastas, P., and Kamenetsky, V.S. (2001) The Palaeoproterozoic komatiite-picrite association of Finnish Lapland. Journal of Petrology, 42, 855-876.

Hauri, E.H., Zhang, J., Herzberg, C., and Fei, Y. (1996) Trace element partitioning at high pressures: new ion probe results and implications for differentiation of a terrestrial magma ocean. Journal of Conference Abstracts 1, 241.

Herzberg, C. (1992) Depth and degree of melting of komatiite. Journal of Geophysical Research, 97, 4521-4540.

Herzberg, C., Condie, K.C., and Korenaga, J. (2010) Thermal history of the Earth and its petrological expression. Earth and Planetary Science Letters, 292, 79-88.

Herzberg, C.T., and O'Hara, M.J. (1985) Origin of mantle peridotite and komatiite by partial melting. Geophysical Research Letters, 12, 541-544.

Hoatson, D.M., Sun, S.-S., Duggan, M.B., Davies, M.B., Daly, S.J., Purvis, A.C. (2005) Late Archean Lake Harris Komatiite, Central Gawler Craton, South Australia: Geologic setting and geochemistry. Economic Geology, 100, 349-374.

Hoffmann, A., and Bohlar, R. (2007) The origin of carbonaeous cherts in the Barberton greenstone belt and their significance for the study of early life in mid-Arcahean rocks. Astrobiology, 7, 355-388.

Hoffmann, A., and Wilson, A. (2007) Silicified basalts, bedded cherts and other sea floor alteration phenomena of the 3.4 Ga Nondweni greenstone belt, South Africa, in: Van Kranendonk, M.J., Smithies, R.H., Bennett, V.C. (Eds.), Earth's Oldest Rocks: Developments in Precambrian Geology. Elsevier, Amsterdam, pp. 571-605.

Irifune, T., and Tsuchiya, T. (2007) Mineralogy of the Earth – Phase transitions and mineralogy of the lower mantle, in: Schubert, G. (Ed.), Treatise on Geophysics, pp. 33-57.

Kröner, A., Hegner, E., Wendt, J.I., and Byerly, G.R. (1996) The oldest part of the Barberton granitoid-greenstone terrain, South Africa: evidence for crust formation between 3.5 and 3.7 Ga. Precambrian Research, 78, 105-124.

Lahaye, Y., and Arndt, N.T. (1996) Alteration of a komatiitic flow: Alexo, Ontario, Canada. Journal of Petrology, 37, 1261-1284.

Lahaye, Y., Arndt, N.T., Byerly, G., Gruau, G., Fourcade, S., and Chauvel, C. (1995) The influence of alteration on the trace-element and Nd isotope compositions of komatiites. Chemical Geology, 126, 43-64.

Lecuyer, C., Gruau, G., Anhaeusser, C.R., and Fourcade, S. (1994) The origin of fluids and the effects of metamorphism on the primary chemical compositions of Barberton komatiites: New evidence from geochemical (REE) and isotopic (Nd, O, H, $^{39}Ar/^{40}Ar$) data. Geochimica et Cosmochimica Acta, 58, 969-984.

Ledevin, M., 2013. Etude géochimique et pétrologique des cherts Archéens de la Ceinture de Roches Vertes de Barberton (3.5-3.2 Gy), Afrique du Sud : Processus de formation et environnement Archéen. University of Grenoble, pp. 323.

Lesher, C.M., and Arndt, N.T. (1995) REE and Nd isotope geochemistry, petrogenesis and volcanic evolution of contaminated komatiites at Kambalda, Western Australia. Lithos, 34, 127-158.

Lowe, D.R., and Byerly, G.R. (2007) An overview of the geology of the Barberton Greenstone Belt and vicinity: Implications for early crustal development, in: Van Kranendonk, M.J., Smithies, R.H., Bennett, V.C. (Eds.), Earth's Oldest Rocks. Elsevier, Amsterdam, pp. 481–526.

Lugmair, G.W., and Marti, K. (1978) Lunar initial $^{143}Nd/^{144}Nd$ differential evolution of the lunar crust and mantle. Earth and Planetary Science Letters, 39, 349-357.

Machado, N., Brooks, C., and Hart, S.R. (1986) Determination of initial $^{87}Sr/^{86}Sr$ and $^{143}Nd/^{144}Nd$ in primary minerals from mafic and ultramafic rocks: experimental procedure and implications for the isotopic characteristics of the Archean mantle under the Abitibi greenstone belt. Geochimica et Cosmochimica Acta, 50, 2335-2348.

McDonough, W.F., and Sun, S.-s. (1995) The composition of the Earth. Chemical Geology, 120, 223-253.

Minster, J.-F., Ricard, L.-P., and Allègre, C.J. (1979) ^{87}Rb-^{87}Sr chronology of enstatite meteorites. Earth and Planetary Science Letters, 44, 420-440.

Nesbitt, R.W., Sun, S.S., and Purvis, A.C. (1979) Komatiites: geochemistry and genesis. Canadian Mineralogist, 17, 165-186.

Ohtani, E., Moriyama, J., and Kawabe, I. (1988) Majorite garnet stability and its implication for genesis of komatiite magmas. Chemical Geology, 70, 147.

Patchett, P.J., White, W.M., Feldmann, H., Kielinczuk, S., and Hofmann, A.W. (1984) Hafnium/rare earth element fractionation in the sedimentary system and crustal recycling into the Earth's mantle. Earth and Planetary Science Letters, 69, 365-378.

Puchtel, I.S., Blichert-Toft, J., Touboul, M., Walker, R.J., Byerly, G.R., Nisbet, E.G., and Anhaeusser, C.R. (2013) Insights into early Earth from Barberton komatiites: Evidence from lithophile isotope and trace element systematics. Geochimica et Cosmochimica Acta, 108, 63-90.

Puchtel, I.S., Hofmann, A.W., Amelin, Y.V., Garbe-Schönberg, C.-D., Samsonov, A.V., and Shchipansky, A.A. (1999) Combined mantle plume-island arc model for the formation of the 2.9 Ga Sumozero-Kenozero greenstone belt, SE Baltic Shield: Isotope and trace element constraints. Geochimica et Cosmochimica Acta, 63, 3579-3595.

Puchtel, I.S., Hofmann, A.W., Mezger, K., Jochum, K.P., Shchipansky, A.A., and Samsonov, A.V. (1998) Oceanic plateau model for continental crustal growth in the Archaean: A case study from the Kostomuksha greenstone belt, NW Baltic Shield. Earth and Planetary Science Letters, 155, 57-74.

Puchtel, I.S., Humayan, M., and Walker, R.J. (2007) Os–Pb–Nd isotope and highly siderophile and lithophile trace element systematics of komatiitic rocks from the Volotsk suite, SE Baltic Shield. Precambrian Research, 158, 119-137.

Puchtel, I.S., Walker, R.J., Touboul, M., Nisbet, E.G., and Byerly, G.R. (2014) Insights into early Earth from the Pt-Re-Os isotope and highly siderophile element abundance systematics of Barberton komatiites. Geochimica et Cosmochimica Acta, 125, 394-413.

Révillon, S., Chauvel, C., Arndt, N.T., Pik, R., Martineau, F., Fourcade, S., and Marty, B. (2002) Heterogeneity of the Caribbean plateau mantle source: new constraints from Sr, O and He isotope compositions of olivine and clinopyroxene. Earth and Planetary Science Letters, 205, 91-106.

Robin-Popieul, C.C.M., Arndt, N.T., Chauvel, C., Byerly, G.R., Sobolev, A.V., and Wilson, A. (2012) A new model for Barberton komatiites: deep critical melting with high melt retention. Journal of Petrology, 53, 2191-2229.

Scherer, E., Münker, C., and Mezger, K. (2001) Calibration of the lutetium-hafnium clock. Science, 293, 683-687.

Söderlund, U., Patchett, P.J., Vervoort, J.D., and Isachsen, C.E. (2004) The ^{176}Lu decay constant determined by Lu-Hf and U-Pb isotope systematics of Precambrian mafic intrusions. Earth and Planetary Science Letters, 219, 311-324.

Sun, S.S., and Nesbitt, R.W. (1978) Petrogenesis of Archean ultrabasic and basic volcanics: evidence from rare earth elements. Contributions to Mineralogy and Petrology, 65, 301-325.

Thompson, P.M.E., Kempton, P.D., White, R.V., Kerr, A.C., Tarney, J., Saunders, A.D., Fitton, J.G., and McBirney, A. (2004) Hf-Nd isotope constraints on the origin of the Cretaceous Caribbean plateau and its relationship to the Galapagos plume. Earth and Planetary Science Letters, 217, 59-75.

Vervoort, J.D., and Blichert-Toft, J. (1999) Evolution of the depleted mantle: Hf isotope evidence from juvenile rocks through time. Geochimica et Cosmochimica Acta, 63, 533-556.

Vervoort, J.D., Patchett, P.J., Blichert-Toft, J., and Albarède, F. (1999) Relationships between Lu-Hf and Sm-Nd isotopic systems in the global sedimentary system. Earth and Planetary Science Letters, 168, 79-99.

Viljoen, M.J., and Viljoen, R.P. (1969) The geology and geochemistry of the lower ultramafic unit of the Onverwacht Group and a proposed new class of igneous rocks. Geological Society of South Africa, Special Publication, 21, 55-85.

Walter, M.J. (1998) Melting of garnet peridotite and the origin of komatiites and depleted lithosphere. Journal of Petrology, 39, 29-60.

Wasserburg, G.J., Jacobsen, S.B., DePaolo, D.J., McCulloch, M.T., and Wen, T. (1981) Precise determination of Sm/Nd ratio, Sm and Nd isotopic abundances in standard solutions. Geochimica et Cosmochimica Acta, 59, 4267-4277.

Wilson, A.H. (2003) A new class of silica enriched, highly depleted komatiites in the southern Kaapvaal Craton, South Africa. Precambrian Research, 127, 125-141.

Wilson, A.H., and Carlson, R.W. (1989) A Sm-Nd and Pb isotopic study of Archaean greenstone belts in the southern Kaapvaal Craton, South Africa. Earth and Planetary Science Letters, 96, 89-105.

Xie, Q., and Kerrich, R. (1994) Silicate-perovskite and majorite signature komatiites from the Archean Abitibi Greenstone belt: Implications for early mantle differentiation and stratification. Journal of Geophysical Research, 99, 15799-15812.

Table captions

Table 1. Lu-Hf and Sm-Nd isotope data for komatiites from Barberton Greenstone Belt drill cores, surface samples, and mineral separates.

Table 2. Parameters used to model the incorporation of chert into komatiite.

Figure captions

Figure 1. Compilation of (a) initial ε_{Nd} and (b) initial ε_{Hf} for komatiites as a function of their age. The youngest 90 Ma komatiites from Gorgona Island are not shown as too far off the x-axis scale. The Nd isotope data are from this study and (Arndt et al. 2001; Arndt et al. 1997; Barrie and Shirey 1991; Chauvel et al. 1987; Chauvel et al. 1993; Chavagnac 2004; Hanski et al. 2001; Hoatson et al. 2005; Lahaye and Arndt 1996; Lahaye et al. 1995; Lecuyer et al. 1994; Lesher and Arndt 1995; Puchtel et al. 2013; Puchtel et al. 1999; Puchtel et al. 1998; Puchtel et al. 2007; Révillon et al. 2002; Wilson and Carlson 1989; Xie and Kerrich 1994). The Hf isotope data are from this study and Blichert-Toft and Arndt (1999), Blichert-Toft et al. (2004), Blichert-Toft and Puchtel (2010), and Puchtel et al. (2013).

Figure 2. $(Gd/Yb)_N$ versus Al_2O_3/TiO_2 for Al-depleted, intermediate, and high-Al komatiites. Data from Robin-Popieul et al. (2012), Coetzee (2014), and Wilson et al. (in preparation).

Figure 3. Summary of the three main types of komatiite found among the surface samples from the Barberton Greenstone Belt analyzed here (Robin-Popieul et al. 2012): (a) Al-depleted or classical Barberton-type komatiites, which have relatively low Al_2O_3/TiO_2 ratios coupled with relative depletion of the HREE; (b) samples with intermediate Al_2O_3/TiO_2 ratios and nearly flat REE patterns; and (c) samples with high Al_2O_3/TiO_2 ratios and strongly sloping LREE-depleted patterns. The trace element patterns of samples from the lower differentiated komatiite sequence plotted in panel (a) show the same features as those illustrated in the sketch of Fig. 10. Data from Robin-Popieul et al. (2012), Coetzee (2014), and Wilson et al. (in preparation).

Figure 4. General geological map of the Barberton Greenstone Belt showing the locations where the samples analyzed in this study were collected.

Figure 5. Geological map showing the locations of outcrop samples collected from the drill site and analyzed in this study, and the locations of the two drill holes that yielded the BARB1 and BARB2 cores. From Robin-Popieul et al. (2012).

Figure 6. Simplified lithological logs of drill cores BARB1 and BARB2 also showing the positions of the samples analyzed in this study.

Figure 7. Lu-Hf isochron diagram for BARB1 and BARB2 whole-rocks, nearby surface samples from the Komati Formation (Grace's Fow), and clinopyroxene separates from several of these. WR = whole-rock; cpx = clinopyroxene.

Figure 8. Sm-Nd isochron diagram for BARB1 and BARB2 whole-rocks, nearby surface samples from the Komati Formation (Grace's Flow), and clinopyroxene and amphibole separates from several of these. WR = whole-rock; cpx = clinopyroxene; amph = amphibole.

Figure 9. Photomicrographs of the olivine cumulates used for the clinopyroxene separations. (a) Image in plane light and (b) under crossed polars of sample GC1. (c) Image in plane light and (d) under crossed polars of sample GC2. Abbreviations: Ol – olivine; sOl – serpentinized olivine; Cpx – clinopyroxene. Partly to completely serpentinized olivine is enclosed by unaltered intercumulus clinopyroxene derived from crystallization of the interstitial melt. The dark cores of the serpentinized olivine in (c) reflect the original compositional zoning in the olivine crystals. These images show textures that indicate that clinopyroxene is a primary magmatic phase that crystallized interstitially to the cumulus olivine, now variably serpentinized

Figure 10. Sketch of the trace element pattern of a source that produces low Sm/Nd and high Lu/Hf.

Figure 11. Cartoon of the effects of fractionation of magnesiowüstite on Lu-Hf and Sm-Nd isotope systematics.

Figure 12. Cartoon showing the "zircon effect". DM = Depleted mantle; CC = Continental crust; PS = Pelagic sediments (i.e. fine-grained deep-sea sediment or chert).

Figure 13. Frequency histogram of the Hf/Sm ratios of the samples analyzed in this study and those of Puchtel et al. (2013). The Hf/Sm ratios of komatiites, whether core or surface samples, and clinopyroxene from the Komati Formation are significantly lower than the CHUR value, while komatiites from the Hooggenoeg and Weltevreden Formations have Hf/Sm ratios within the uncertainties of CHUR. This suggests the presence of a fine-grained

910 sedimentary component in the source of the Komati Formation lavas but not in those of the Hooggenoeg and Weltevreden Formation lavas. WR = whole-rock; cpx = clinopyroxene; Fm = Formation.

Table 1. Lu-Hf and Sm-Nd isotope data for komatiites from Barberton Greenstone Belt drill cores, surface samples, and mineral separates.

Sample name	Other name	Rock type/mineral	Depth (m)	Age T (Ma)	Hf (ppm)	Lu (ppm)	176Lu/177Hf	176Hf/177Hf	±2 sigma	(176Hf/177Hf)T	εHf(T)	±2 sigma	Nd (ppm)	Sm (ppm)	147Sm/144Nd	143Nd/144Nd	±2 sigma	(143Nd/144Nd)T	εNd(T)	±2 sigma	Hf/Sm
Core samples (Komati Formation)																					
BARB1																					
BARB1-10.18	GC/1	Ol cumulate	10.18	3480	0.121	0.0262	0.03075	0.282647	0.000006	0.280583	1.4	0.3	0.806	0.232	0.1738	0.512149	0.000004	0.508148	0.8	0.3	0.52
BARB1-31.29	GC/17	Ol cumulate- harrisite	31.29	3480	0.175	0.0344	0.02793	0.282471	0.000007	0.280596	1.9	0.3	0.993	0.303	0.1846	0.512420	0.000005	0.508169	1.2	0.3	0.58
BARB1-44.03	GC/3	Harrisite	44.03	3480	0.233	0.0450	0.02744	0.282342	0.000011	0.280500	-1.6	0.4	1.37	0.392	0.1736	0.512158	0.000005	0.508162	1.0	0.3	0.59
BARB1-54.38	GC/4	Px spinifex	54.38	3480	1.15	0.199	0.02462	0.282251	0.000003	0.280598	2.0	0.2	6.51	1.91	0.1777	0.512208	0.000005	0.508119	0.2	0.3	0.60
BARB1-58.5	GC/5	Pyroxenite	58.50	3480	0.968	0.173	0.02544	0.282293	0.000006	0.280585	1.5	0.2	5.35	1.61	0.1819	0.512298	0.000004	0.508110	0.0	0.3	0.60
BARB1-62.92	GC/7	Px spinifex	62.92	3480	1.14	0.195	0.02420	0.282209	0.000004	0.280584	1.5	0.2	6.36	1.87	0.1777	0.512211	0.000006	0.508121	0.2	0.3	0.61
BARB1-85.72	GC/34A	Hyaloclastite-block	85.72	3480	0.511	0.0677	0.01881	0.281915	0.000003	0.280652	3.9	0.2	2.21	0.636	0.1737	0.512207	0.000004	0.508208	1.9	0.3	0.80
BARB1-89.23	GC/9	Hyaloclastite	89.23	3480	0.627	0.107	0.02431	0.282244	0.000004	0.280612	2.4	0.2	3.37	1.01	0.1806	0.512227	0.000006	0.508070	-0.8	0.3	0.62
BARB1-104.77	AHW/DM/9	Ol cumulate	104.77	3480	0.266	0.0638	0.03401	0.282737	0.000006	0.280454	-3.2	0.3	2.25	0.684	0.1841	0.512459	0.000004	0.508222	2.2	0.3	0.39
BARB1-105.52	AHW/DM/11	Harrisite	105.52	3480	0.363	0.0731	0.02855	0.282434	0.000010	0.280517	-0.9	0.4	2.52	0.748	0.1797	0.512181	0.000007	0.508044	-1.3	0.3	0.49
BARB1-108.71	AHW/DM/13	Ol spinifex	108.71	3480	0.644	0.116	0.02551	0.282294	0.000003	0.280581	1.3	0.2	3.84	1.10	0.1728	0.511970	0.000004	0.507993	-2.3	0.3	0.59
BARB1-391.435	AHW/TM/15	Ol cumulate	391.44	3480	0.507	0.105	0.02929	0.282526	0.000010	0.280560	0.6	0.4	3.46	1.10	0.1923	0.512577	0.000006	0.508149	0.8	0.3	0.46
BARB1-398.54	AHW/TM/21	Ol cumulate	398.54	3480	0.368	0.0689	0.02656	0.282428	0.000046	0.280644	3.6	1.6	1.93	0.626	0.1961	0.512650	0.000006	0.508137	0.5	0.3	0.59
BARB1-402.48	AHW/TM/25	Vesicles	402.48	3480	0.407	0.0720	0.02512	0.282302	0.000009	0.280615	2.6	0.3	2.04	0.661	0.1963	0.512599	0.000004	0.508080	-0.6	0.3	0.61
BARB1-410.445	AHW/TM/35	Ol spinifex	410.45	3480	0.781	0.135	0.02447	0.282251	0.000008	0.280608	2.3	0.3	3.42	1.11	0.1954	0.512691	0.000003	0.508193	1.6	0.3	0.71
BARB2																					
BARB2-252.60	BARB 2 GC/1	Chill	252.60	3480	0.577	0.112	0.02758	0.282447	0.000005	0.280595	1.8	0.2	3.33	1.09	0.1972	0.512735	0.000004	0.508195	1.7	0.3	0.53
BARB2-254.50	BARB 2 GC/3	Ol cumulate	254.50	3480	0.364	0.0662	0.02578	0.282326	0.000008	0.280595	1.8	0.3	2.14	0.660	0.1867	0.512453	0.000005	0.508155	0.9	0.3	0.55
BARB2-257.66	BARB 2 GC/6	Ol spinifex	257.66	3480	0.661	0.122	0.02616	0.282341	0.000004	0.280585	1.5	0.2	3.56	1.18	0.2007	0.512735	0.000009	0.508115	0.1	0.3	0.56
Outcrop samples from Grace's Flow (a thick komatiite flow at the base of BARB2)																					
GC1		Ol cumulate		3480	0.715	0.0884	0.01754	0.281873	0.000008	0.280696	5.4	0.3	2.22	0.920	0.2504	0.513779	0.000005	0.508014	-1.9	0.3	0.78
GC2		Ol cumulate		3480	0.737	0.0934	0.01798	0.281882	0.000006	0.280675	4.7	0.2	2.36	0.946	0.2425	0.513596	0.000004	0.508013	-1.9	0.3	0.78
PXITE		Cpx cumulate		3480	1.05	0.138	0.01863	0.281918	0.000004	0.280667	4.4	0.2	3.63	1.39	0.2310	0.513414	0.000005	0.508095	-0.3	0.3	0.76
BD1		Ol cumulate		3480	0.337	0.0581	0.02448	0.282307	0.000006	0.280664	4.3	0.2	2.012	0.581	0.1746	0.512250	0.000005	0.508230	2.4	0.3	0.58
BD2		Ol cumulate		3480	0.763	0.135	0.02518	0.281864	0.000005	0.280174	-13.2	0.2	2.500	0.988	0.2389	0.513585	0.000004	0.508085	-0.5	0.3	0.77
BD4		Ol spinifex		3480	0.603	0.101	0.02379	0.282424	0.000050	0.280827	10.1	1.8	3.386	0.998	0.1781	0.512229	0.000005	0.508129	0.4	0.3	0.60
BD18		Ol cumulate		3480	0.310	0.0533	0.02444	0.282295	0.000006	0.280654	4.0	0.2	1.738	0.511	0.1776	0.512264	0.000005	0.508175	1.3	0.3	0.61
Mineral separates from outcrop samples from Grace's Flow																					
GC1 cpx1 (attack 1)		Clinopyroxene		3480	0.465	0.137	0.04191	0.283467	0.000008	0.280654	4.0	0.3	1.25	0.671	0.3249	0.515507	0.000007	0.508027	-1.6	0.3	0.69
GC1 cpx1 (attack 2)		Clinopyroxene		3480	0.464	0.134	0.04107	0.283465	0.000009	0.280708	5.9	0.3	1.24	0.665	0.3251	0.515480	0.000006	0.507995	-2.3	0.3	0.70
GC2 cpx2 (attack 1)		Clinopyroxene		3480	0.509	0.132	0.03672	0.283099	0.000007	0.280634	3.2	0.3	1.54	0.795	0.3121	0.515194	0.000005	0.508010	-2.0	0.3	0.64
GC2 cpx2 (attack 2)		Clinopyroxene		3480	0.497	0.130	0.03717	0.283189	0.000007	0.280694	5.4	0.3	1.46	0.750	0.3099	0.515128	0.000006	0.507995	-2.3	0.3	0.66
GC3 cpx3		Clinopyroxene		3480	0.425	0.141	0.04716	0.283779	0.000030	0.280613	2.5	1.1	1.56	0.735	0.2852	0.514783	0.000006	0.508217	2.1	0.3	0.58
GC3 amph		Amphibole (impure)		3480	1.82	0.122	0.00952	0.282055	0.000006	0.281416	31	0.2	2.35	1.12	0.2875	0.514733	0.000005	0.508115	0.1	0.3	
Other outcrop samples (Komati Formation)																					
BD5				3480	0.608	0.142	0.03306	0.282343	0.000005	0.280124	-14.9	0.2	2.987	0.932	0.1886	0.512487	0.000004	0.508145	0.7	0.3	0.65
BD6				3480	0.303	0.0547	0.02566	0.282323	0.000004	0.280600	2.0	0.2	1.670	0.522	0.1888	0.512476	0.000006	0.508129	0.4	0.3	0.58
BD7				3480	1.07	0.181	0.02403	0.282318	0.000025	0.280705	5.8	0.9	5.875	1.793	0.1845	0.512392	0.000004	0.508145	0.7	0.3	0.59
BD11				3480	0.604	0.0961	0.02256	0.282257	0.000005	0.280743	7.1	0.2	3.229	1.013	0.1897	0.512701	0.000005	0.508335	4.4	0.3	0.60
BD12				3480	0.275	0.0468	0.02419	0.282298	0.000006	0.280674	4.7	0.2	1.362	0.441	0.1956	0.512626	0.000006	0.508123	0.3	0.3	0.62
BD20				3480	0.384	0.0714	0.02640	0.282327	0.000004	0.280555	0.4	0.2	1.449	0.562	0.2345	0.513304	0.000005	0.507906	-4.0	0.3	0.68
BD21				3480	0.182	0.0359	0.02793	0.282490	0.000011	0.280615	2.6	0.4	1.200	0.335	0.1689	0.512129	0.000005	0.508242	2.6	0.3	0.54
BD23				3480	0.265	0.0479	0.02561	0.282315	0.000005	0.280596	1.9	0.2	1.301	0.417	0.1937	0.512553	0.000004	0.508094	-0.3	0.3	0.64
SS011				3480	0.183	0.0478	0.03714	0.283088	0.000006	0.280594	1.8	0.2	0.929	0.301	0.1958	0.512632	0.000006	0.508125	0.3	0.3	0.61
SS013				3480	0.173	0.0453	0.03718	0.283093	0.000008	0.280598	1.9	0.3	0.880	0.285	0.1961	0.512648	0.000005	0.508135	0.5	0.3	0.61

SS015	3480	0.143	0.0376	0.03733	0.283116	0.000007	0.280610	2.4	0.3	0.727	0.236	0.1959	0.512657	0.000005	0.508148	0.7	0.3	0.61
Outcrop samples (Hooggenoeg Formation)																		
HOG1	3470									2.450	0.869	0.2145	0.513050	0.000005	0.508127	0.1	0.3	
HOG2	3470	0.652	0.192	0.04190	0.283375	0.000004	0.280571	0.7	0.2	2.665	0.941	0.2134	0.513035	0.000004	0.508136	0.3	0.3	0.69
HOG5	3470	0.328	0.0659	0.02854	0.282554	0.000007	0.280644	3.4	0.3	1.259	0.450	0.2160	0.513101	0.000005	0.508143	0.4	0.3	0.73
Outcrop samples (Weltevreden Formation)																		
MC6-4	3270	0.125	0.104	0.1181	0.283885	0.000021	0.276450	-151	0.8	0.402	0.157	0.2355	0.513506	0.000005	0.508417	0.6	0.2	0.80
MC7-6	3270	0.204	0.0676	0.04711	0.283903	0.000014	0.280937	9.1	0.5	0.671	0.264	0.2381	0.513569	0.000006	0.508422	0.7	0.2	0.77
MC5-1	3270	0.0540	0.0187	0.04906	0.284087	0.000055	0.280999	11.3	2.0	0.197	0.072	0.2225	0.513275	0.000009	0.508465	1.6	0.2	0.75
MC5-3	3270	0.0837	0.0268	0.04553	0.283856	0.000023	0.280990	11.0	0.8	0.289	0.106	0.2213	0.513205	0.000006	0.508422	0.7	0.2	0.79
MC5-5	3270	0.327	0.104	0.04495	0.283742	0.000007	0.280912	8.2	0.3	1.141	0.424	0.2244	0.513278	0.000004	0.508428	0.8	0.2	0.77
MC5-7	3270	0.239	0.0714	0.04241	0.283598	0.000022	0.280928	8.8	0.8	0.868	0.323	0.2246	0.513287	0.000004	0.508431	0.9	0.2	0.74
MC4-3	3270	0.128	0.0370	0.04111	0.283646	0.000010	0.281058	13.4	0.4	0.433	0.159	0.2222	0.513232	0.000005	0.508429	0.8	0.2	0.80
MC4-4	3270	0.0963	0.0308	0.04540	0.283904	0.000017	0.281046	13.0	0.6	0.352	0.130	0.2225	0.513242	0.000005	0.508432	0.9	0.2	0.74
SA719-1	3270	0.215	0.0492	0.03252	0.283013	0.000007	0.280966	10.1	0.3	0.859	0.292	0.2057	0.512882	0.000005	0.508436	1.0	0.2	0.73
SA719-2	3270	0.540	0.117	0.03069	0.282836	0.000003	0.280904	7.9	0.1	2.001	0.681	0.2059	0.512897	0.000005	0.508447	1.2	0.2	0.79
SA719-4	3270	0.165	0.0414	0.03564	0.283149	0.000021	0.280905	8.0	0.8	0.750	0.250	0.2012	0.512759	0.000004	0.508410	0.5	0.2	0.66
WP104	3270	0.160	0.0570	0.05055	0.283981	0.000007	0.280798	4.1	0.3	0.540	0.206	0.2312	0.513436	0.000005	0.508438	1.0	0.2	0.78
WP107	3270	0.205	0.0741	0.05134	0.284024	0.000007	0.280792	3.9	0.3	0.694	0.269	0.2344	0.513491	0.000007	0.508424	0.7	0.2	0.76
WP108	3270	0.578	0.186	0.04560	0.283707	0.000007	0.280836	5.5	0.3	2.052	0.777	0.2290	0.513382	0.000005	0.508431	0.9	0.2	0.74
WP109	3270	0.141	0.0450	0.04518	0.283724	0.000007	0.280880	7.0	0.3	0.479	0.178	0.2243	0.513346	0.000005	0.508498	2.2	0.2	0.80

Table 2. Parameters used to model the incorporation of chert into komatiite.

	Komatiite	Old chert	Mantle
Nd (ppm)	3	3	0.7
Epsi Nd	1	-8	1
Hf (ppm)	1	1	0.17
Epsi Hf	3	8	3
SiO2 (%)	47	100	45

Results	Contaminated komatiite	Source + old chert
% Chert	60	10
% SiO2 in komatiite	78	
% SiO2 in source		50

The SiO2, Nd, and Hf contents are based on the estimated composition of the parental magma of Grace's Flow (Coetzee, 2014). The isotopic compositions are from this study.

The chert elemental and isotopic compositions are from Ledevin (2013) and Garçon et al. (2015 and unpublished data)

The mantle composition is from McDonough and Sun (1995) and Puchtel et al. (2013)

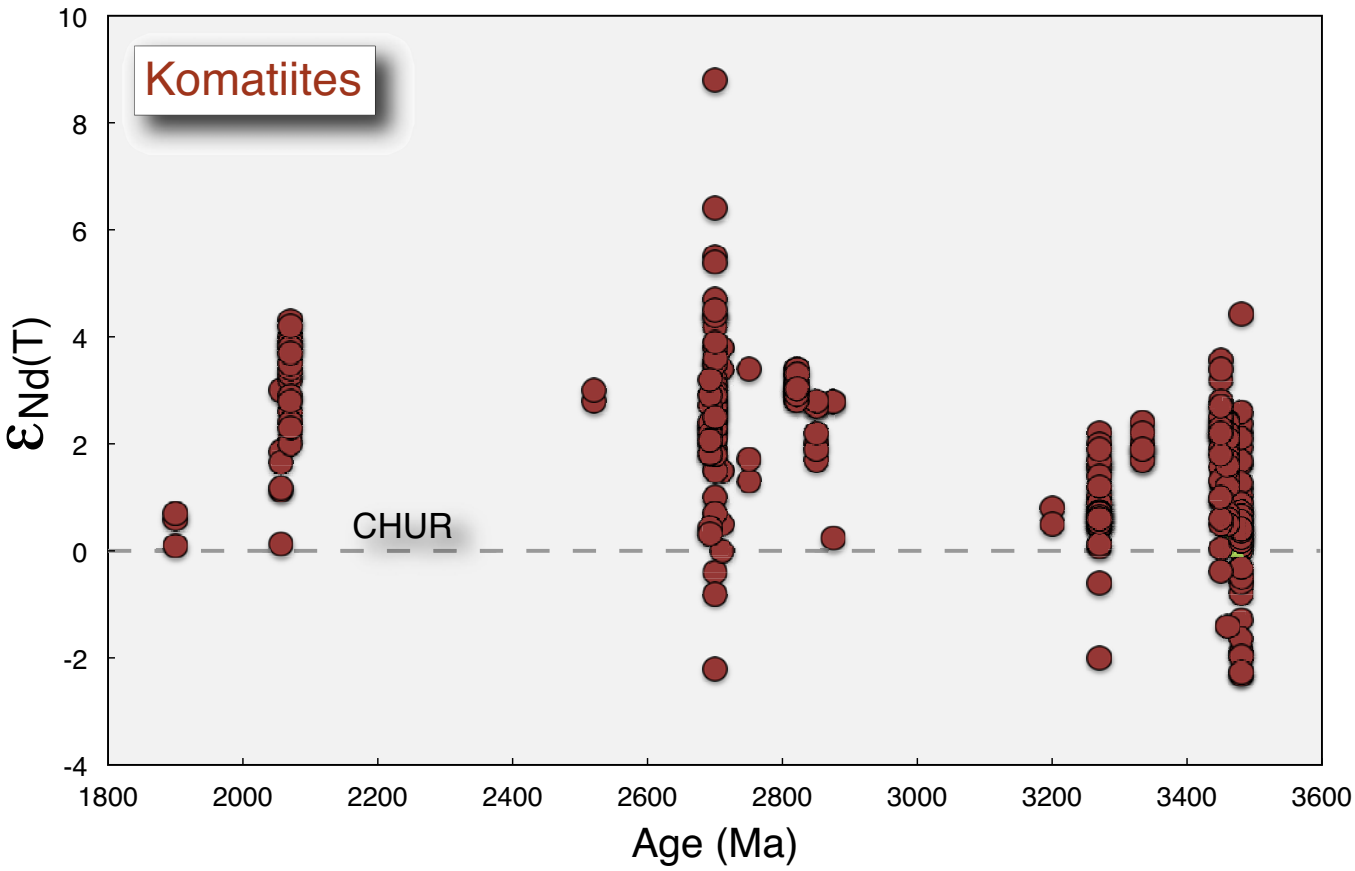
Komatiites
CHUR
εNd(T)
Age (Ma)
10
8
6
4
2
0
-2
-4
1800
2000
2200
2400
2600
2800
3000
3200
3400
3600

Fig. 1a

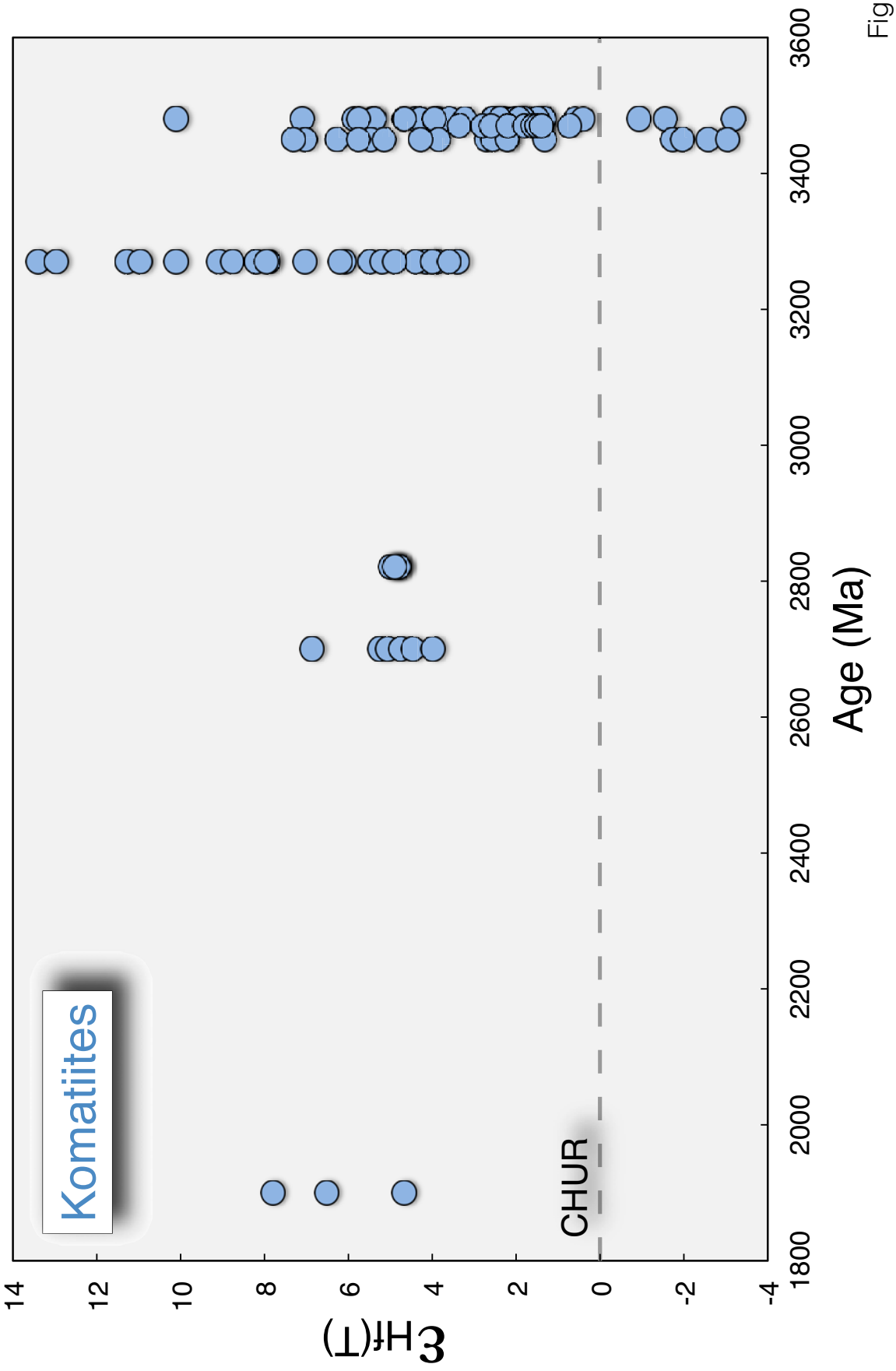
Komatiites
CHUR
εHf(T)
Age (Ma)
14
12
10
8
6
4
2
0
-2
-4
1800
2000
2200
2400
2600
2800
3000
3200
3400
3600

Fig. 1b

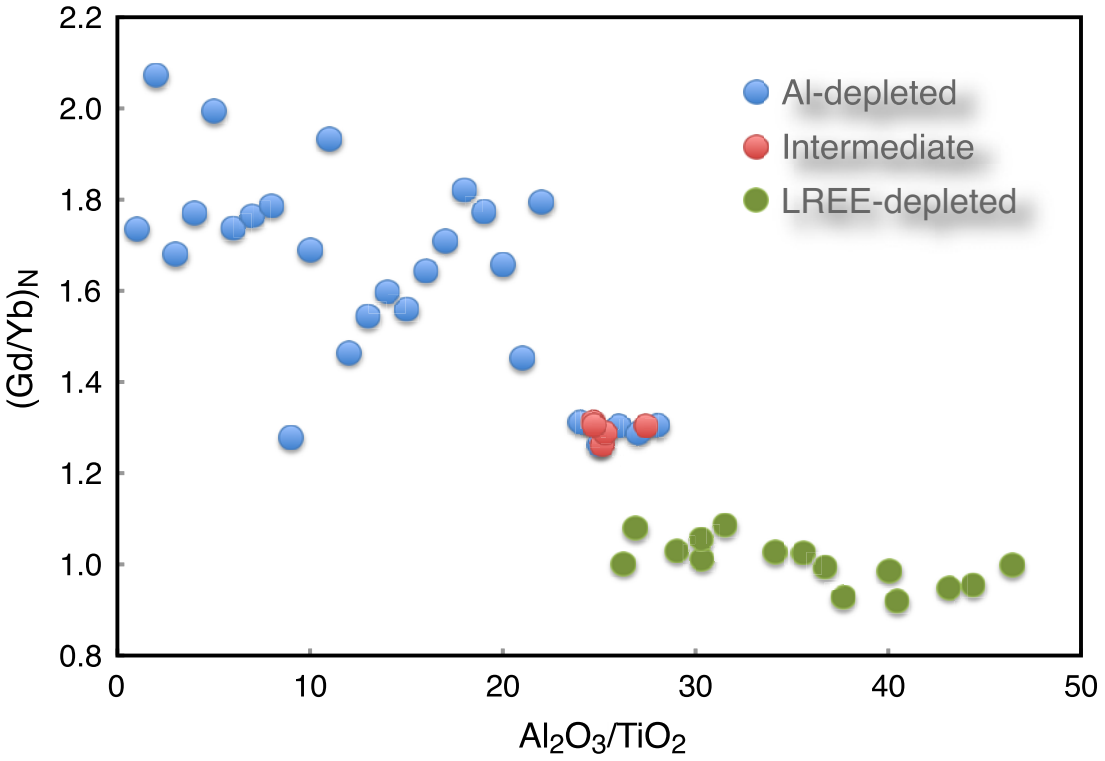
Al-depleted
Intermediate
LREE-depleted
(Gd/Yb)N
Al2O3/TiO2
2.2
2.0
1.8
1.6
1.4
1.2
1.0
0.8
0
10
20
30
40
50

Fig. 2

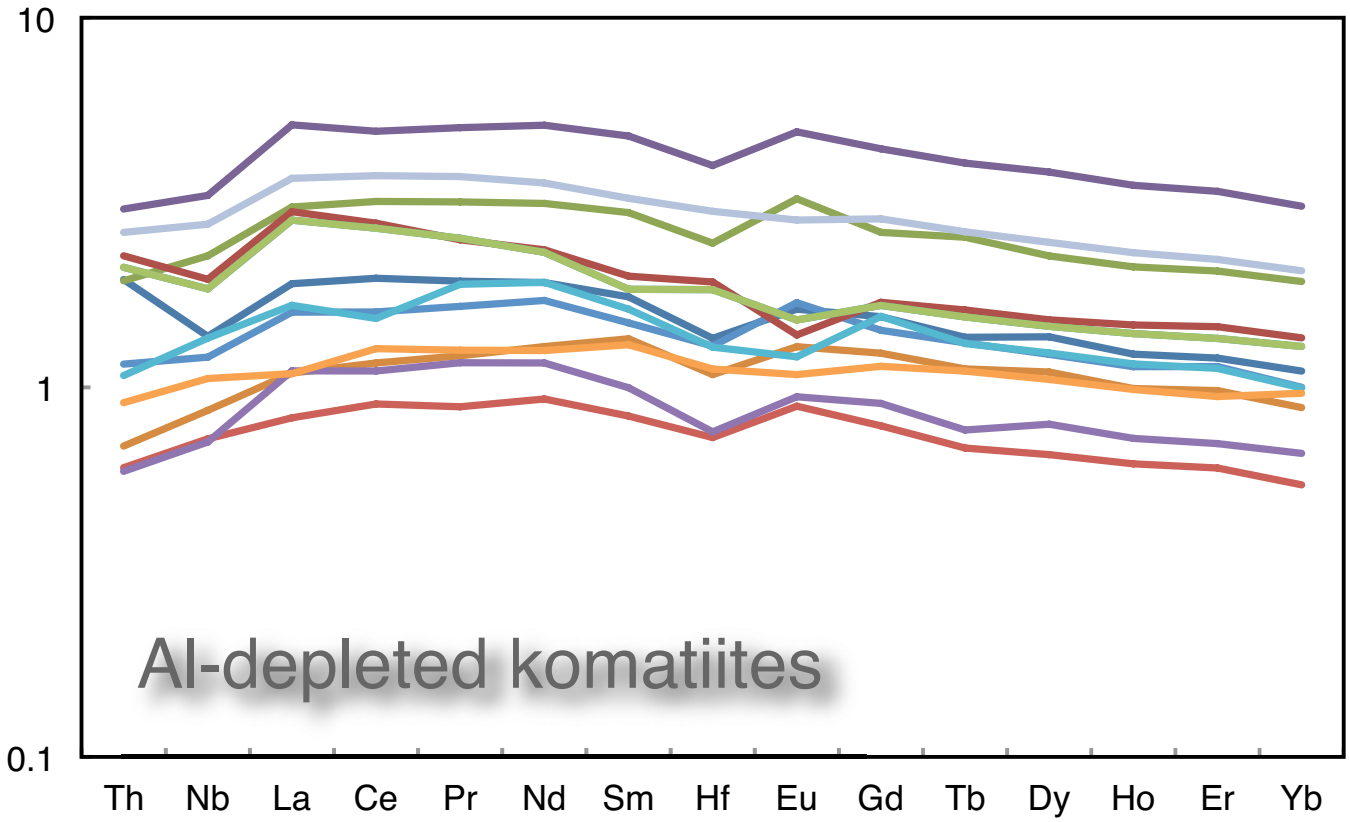
10
1
0.1
Al-depleted komatiites
Th
Nb
La
Ce
Pr
Nd
Sm
Hf
Eu
Gd
Tb
Dy
Ho
Er
Yb

Fig. 3a

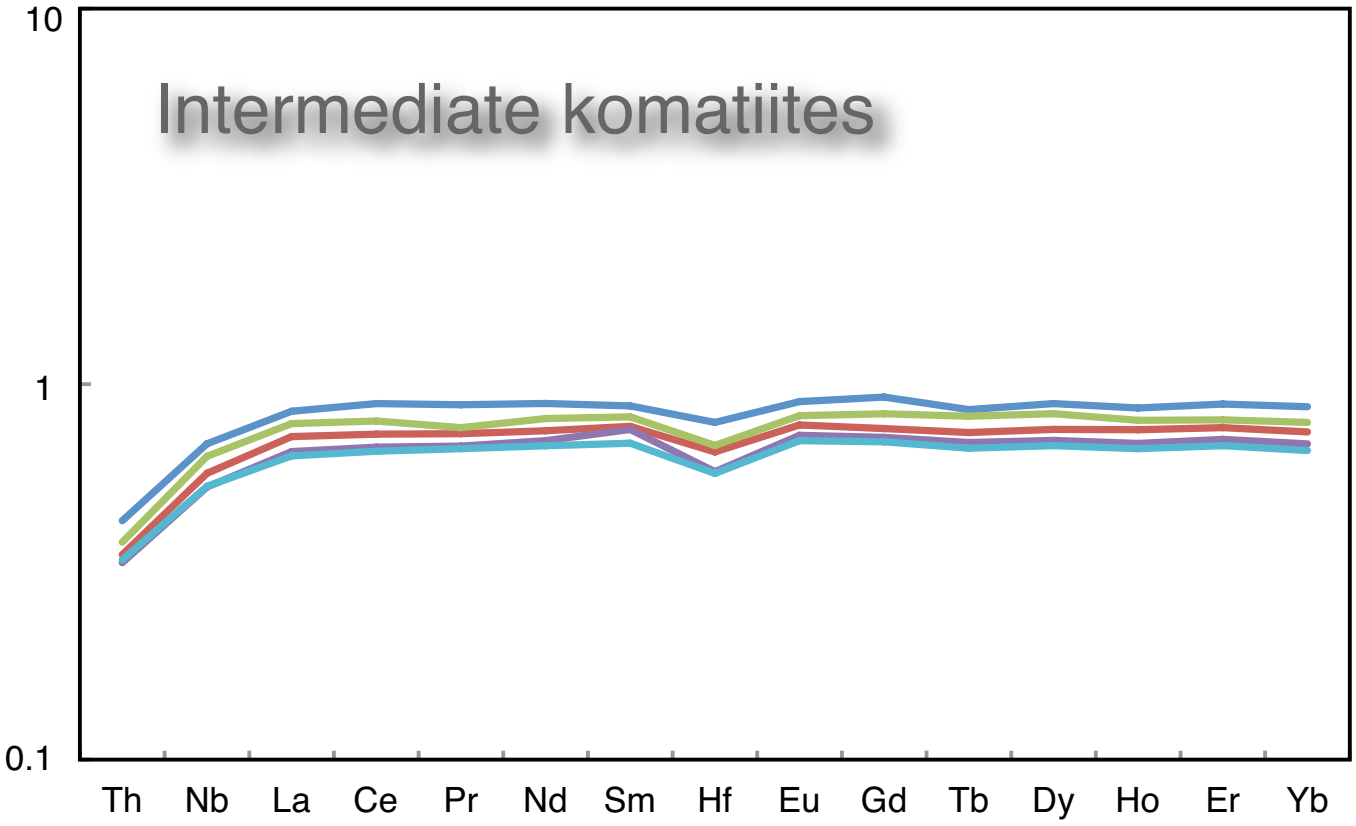
10
1
0.1
Intermediate komatiites
Th
Nb
La
Ce
Pr
Nd
Sm
Hf
Eu
Gd
Tb
Dy
Ho
Er
Yb

Fig. 3b

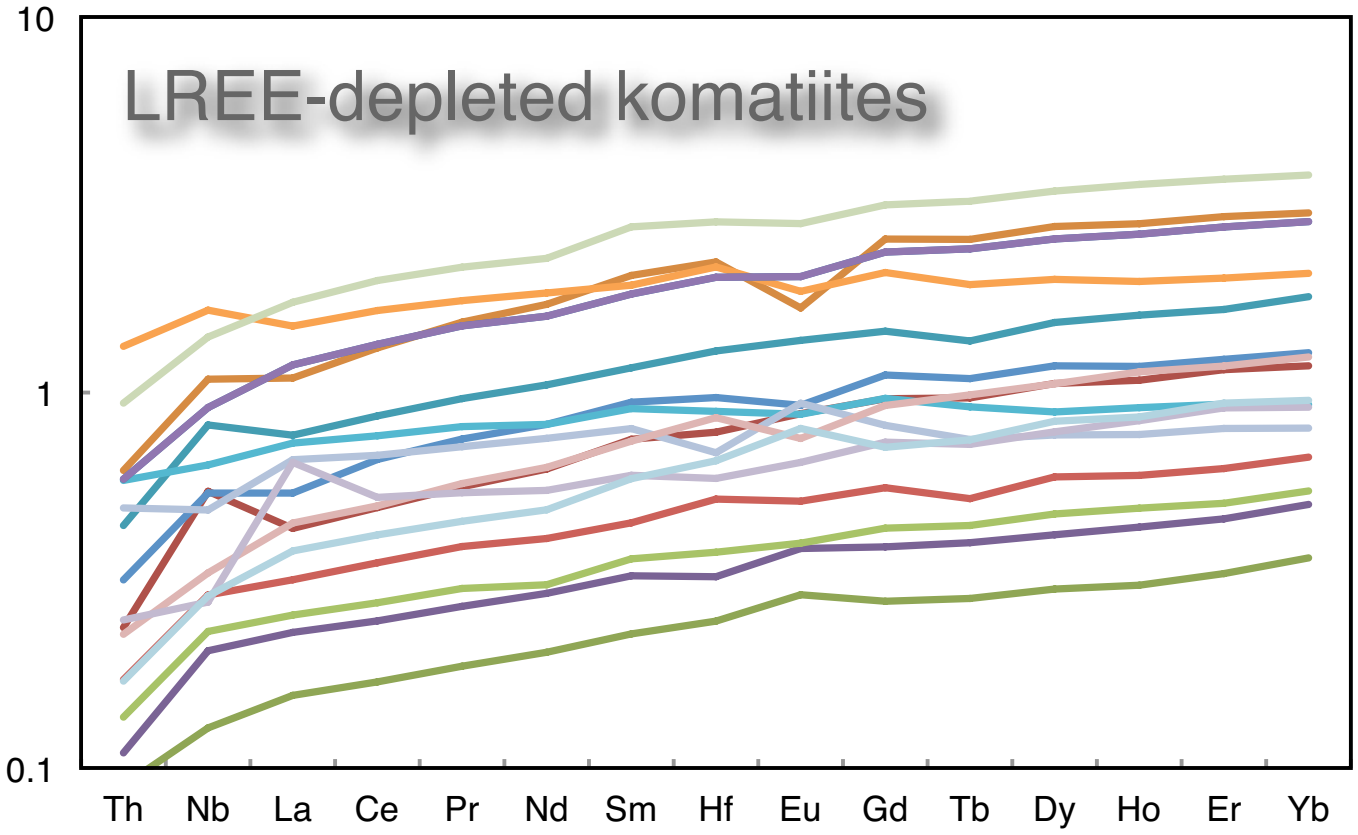
LREE-depleted komatiites
10
1
0.1
Th
Nb
La
Ce
Pr
Nd
Sm
Hf
Eu
Gd
Tb
Dy
Ho
Er
Yb

Fig. 3c

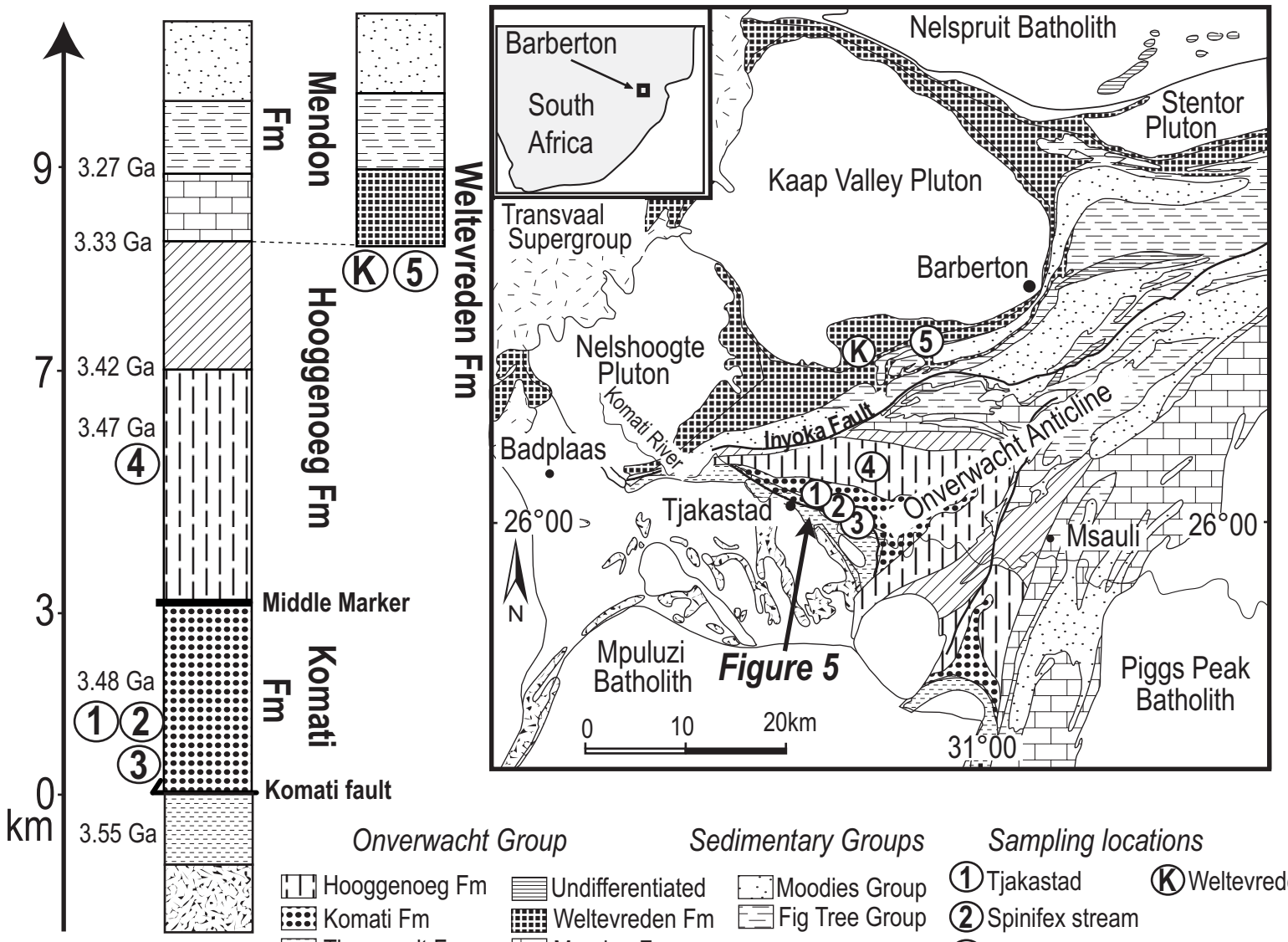
9
7
3
0
km
3.27 Ga
3.33 Ga
3.42 Ga
3.47 Ga
3.48 Ga
3.55 Ga
Mendon Fm
Hooggenoeg Fm
Komati Fm
Weltevreden Fm
Middle Marker
Komati fault
Barberton
South Africa
Nelspruit Batholith
Stentor Pluton
Kaap Valley Pluton
Transvaal Supergroup
Barberton
Nelshoogte Pluton
Komati River
Invoka Fault
Onverwacht Anticline
Badplaas
Tjakastad
Msauli
26°00
31°00
N
Mpuluzi Batholith
Figure 5
Piggs Peak Batholith
0
10
20km
Onverwacht Group
Hooggenoeg Fm
Komati Fm
Theespruit Fm
Sandspruit Fm
Undifferentiated
Weltevreden Fm
Mendon Fm
Kromberg Fm
Sedimentary Groups
Moodies Group
Fig Tree Group
Felsic plutons
Sampling locations
1 Tjakastad
2 Spinifex stream
3 Spinifex horizon 1
4 Hooggenoeg
5 Pioneer complex
K Weltevreden

Fig. 4

Fig. 5

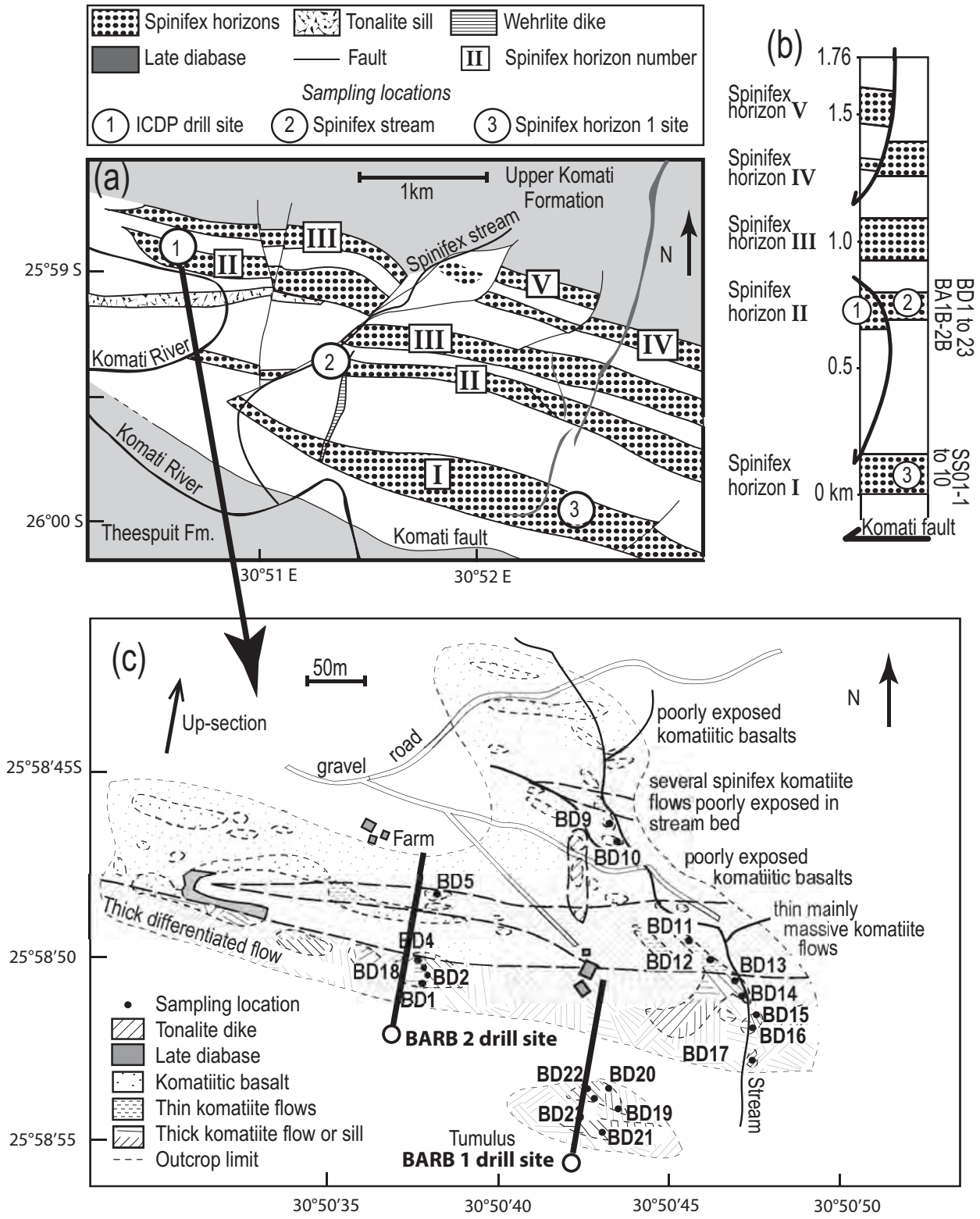
Spinifex horizons
Tonalite sill
Wehrlite dike
Late diabase
Fault
II Spinifex horizon number
Sampling locations
1 ICDP drill site
2 Spinifex stream
3 Spinifex horizon 1 site
(a)
1km
Upper Komati Formation
Spinifex stream
N
25°59 S
26°00 S
Komati River
Komati River
Theespuit Fm.
Komati fault
30°51 E
30°52 E
(b)
1.76
1.5
1.0
0.5
0 km
Spinifex horizon V
Spinifex horizon IV
Spinifex horizon III
Spinifex horizon II
Spinifex horizon I
BD1 to 23 BA1B-2B
SS01-1 to 10
Komati fault
(c)
50m
Up-section
N
poorly exposed komatiitic basalts
road
gravel
several spinifex komatiite flows poorly exposed in stream bed
Farm
BD9
BD10
poorly exposed komatiitic basalts
BD5
thin mainly massive komatiite flows
Thick differentiated flow
BD11
BD4
BD12
BD13
BD18
BD2
BD14
BD1
BD15
BD16
BARB 2 drill site
BD17
BD22
BD20
Stream
BD19
BD21
Tumulus
BARB 1 drill site
25°58′45S
25°58′50
25°58′55
Sampling location
Tonalite dike
Late diabase
Komatiitic basalt
Thin komatiite flows
Thick komatiite flow or sill
Outcrop limit
30°50′35
30°50′40
30°50′45
30°50′50

Fig. 6

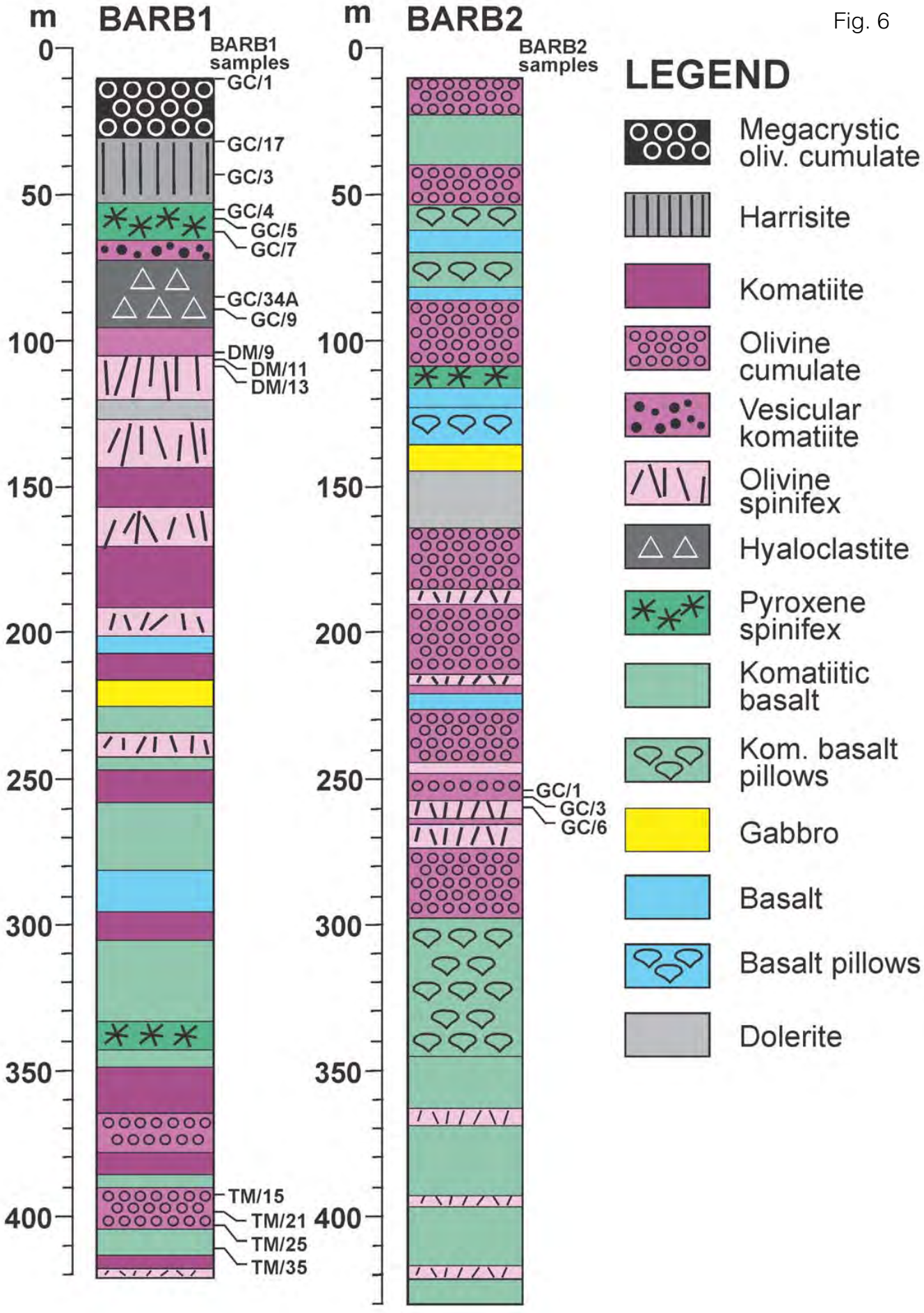
m
BARB1
BARB1 samples
0
50
100
150
200
250
300
350
400
GC/1
GC/17
GC/3
GC/4
GC/5
GC/7
GC/34A
GC/9
DM/9
DM/11
DM/13
TM/15
TM/21
TM/25
TM/35
m
BARB2
BARB2 samples
GC/1
GC/3
GC/6
LEGEND
Megacrystic oliv. cumulate
Harrisite
Komatiite
Olivine cumulate
Vesicular komatiite
Olivine spinifex
Hyaloclastite
Pyroxene spinifex
Komatiitic basalt
Kom. basalt pillows
Gabbro
Basalt
Basalt pillows
Dolerite

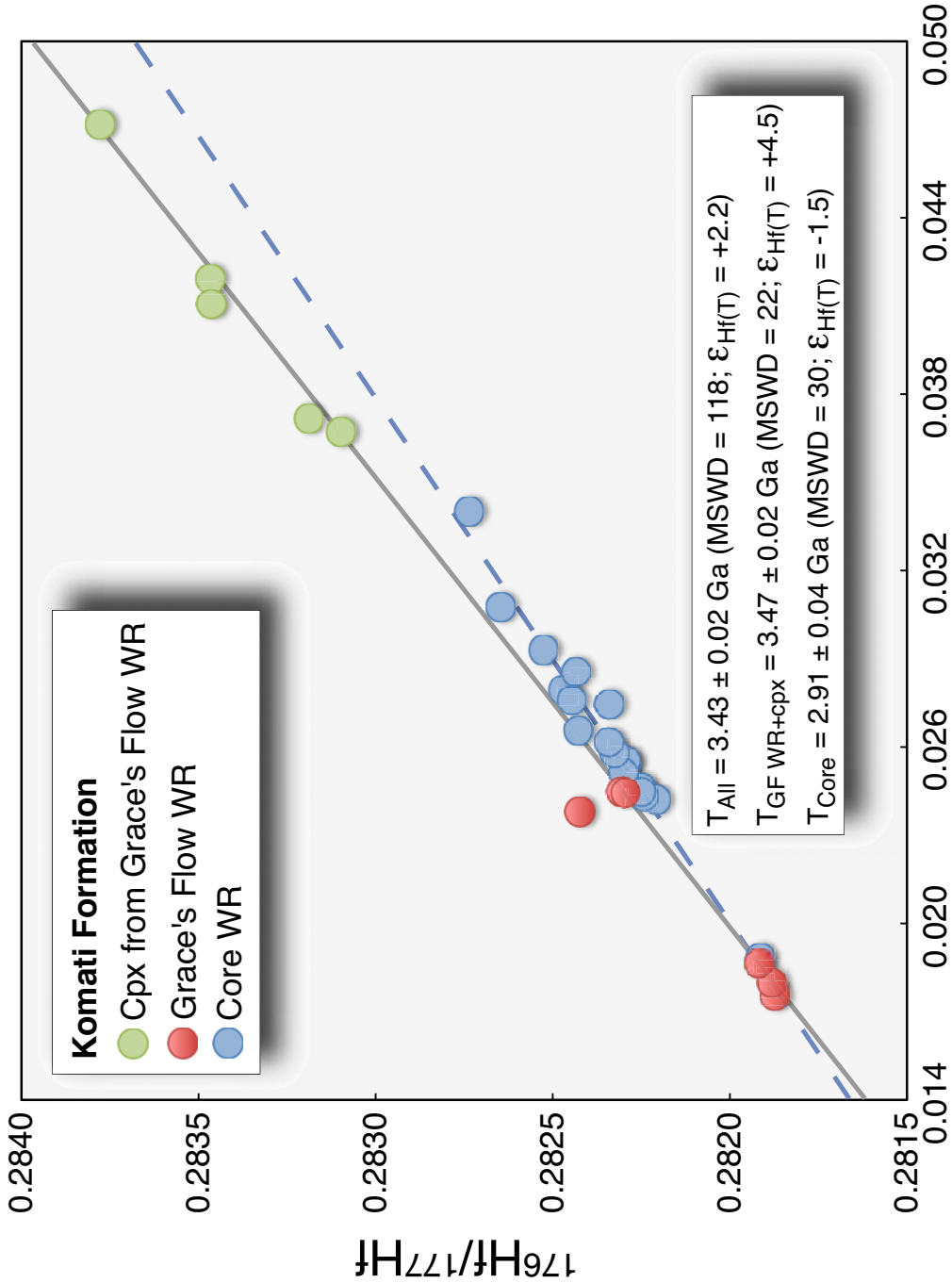
Komati Formation
Cpx from Grace's Flow WR
Grace's Flow WR
Core WR
T_{All} = 3.43 ± 0.02 Ga (MSWD = 118; $\varepsilon_{Hf(T)}$ = +2.2)
$T_{GF\ WR+cpx}$ = 3.47 ± 0.02 Ga (MSWD = 22; $\varepsilon_{Hf(T)}$ = +4.5)
T_{Core} = 2.91 ± 0.04 Ga (MSWD = 30; $\varepsilon_{Hf(T)}$ = -1.5)
$^{176}Hf/^{177}Hf$
$^{176}Lu/^{177}Hf$
0.2840
0.2835
0.2830
0.2825
0.2820
0.2815
0.014
0.020
0.026
0.032
0.038
0.044
0.050

Fig. 7

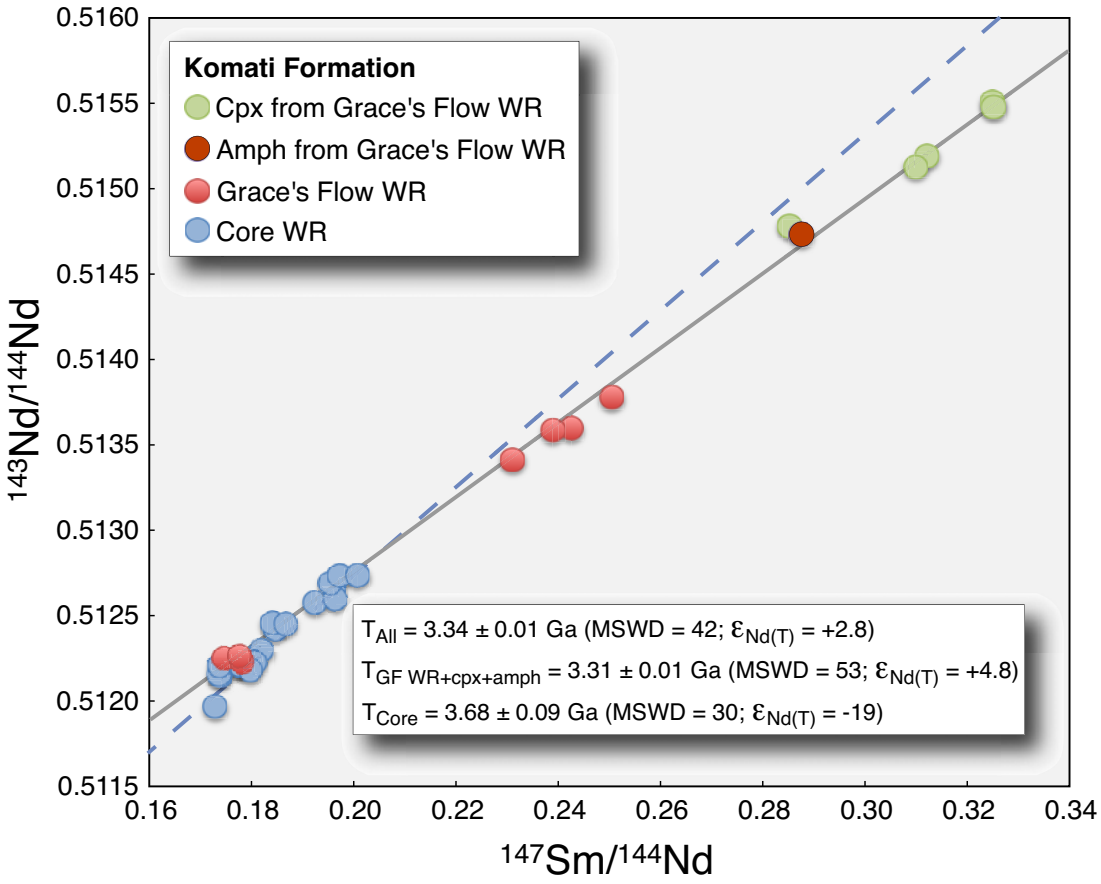
Komati Formation
Cpx from Grace's Flow WR
Amph from Grace's Flow WR
Grace's Flow WR
Core WR
T_All = 3.34 ± 0.01 Ga (MSWD = 42; ε_Nd(T) = +2.8)
T_GF WR+cpx+amph = 3.31 ± 0.01 Ga (MSWD = 53; ε_Nd(T) = +4.8)
T_Core = 3.68 ± 0.09 Ga (MSWD = 30; ε_Nd(T) = -19)
143Nd/144Nd
147Sm/144Nd
0.5160
0.5155
0.5150
0.5145
0.5140
0.5135
0.5130
0.5125
0.5120
0.5115
0.16
0.18
0.20
0.22
0.24
0.26
0.28
0.30
0.32
0.34

Fig. 8

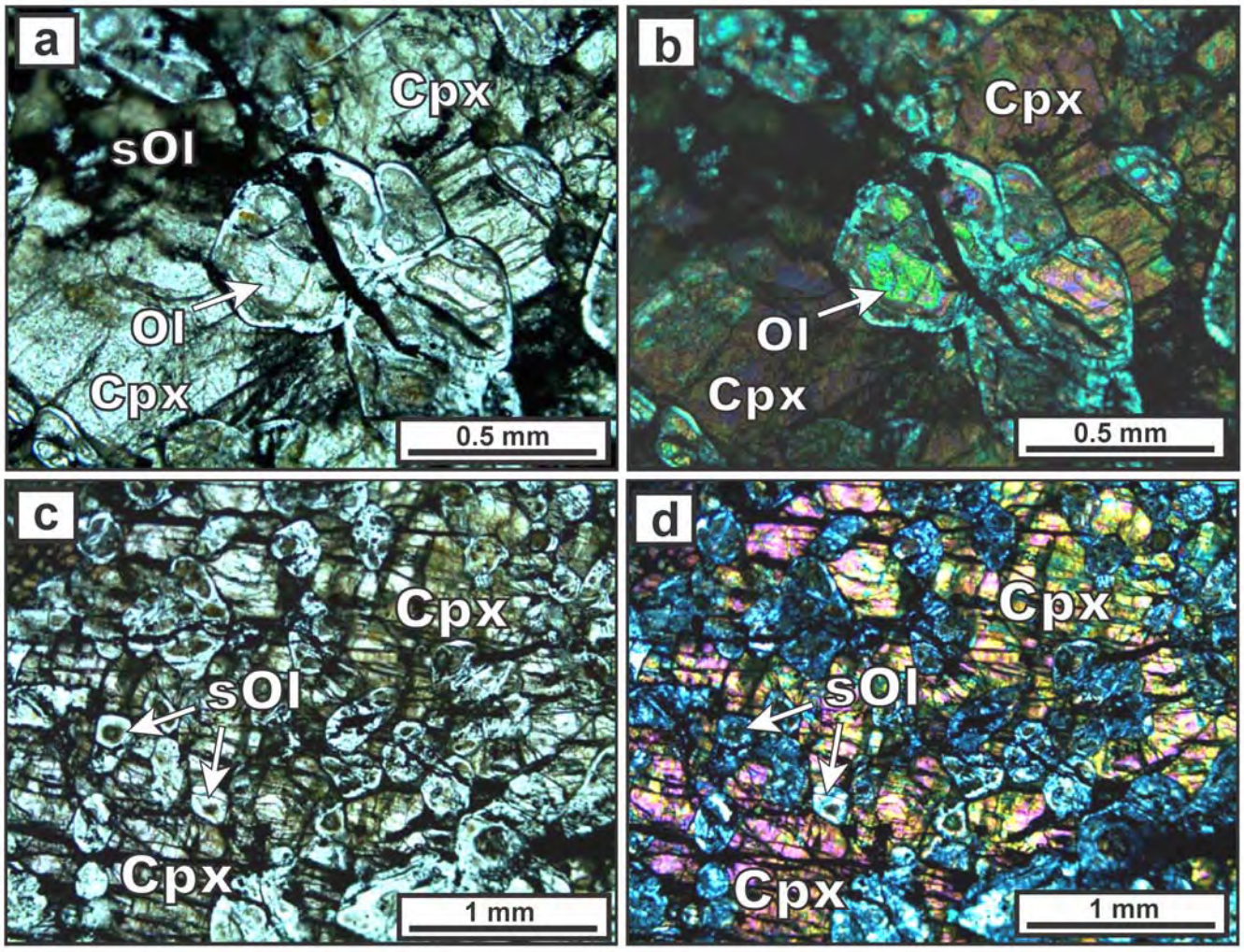
a
Cpx
sOl
Ol
Cpx
0.5 mm
b
Cpx
Ol
Cpx
0.5 mm
c
Cpx
sOl
Cpx
1 mm
d
Cpx
sOl
Cpx
1 mm

Fig. 9

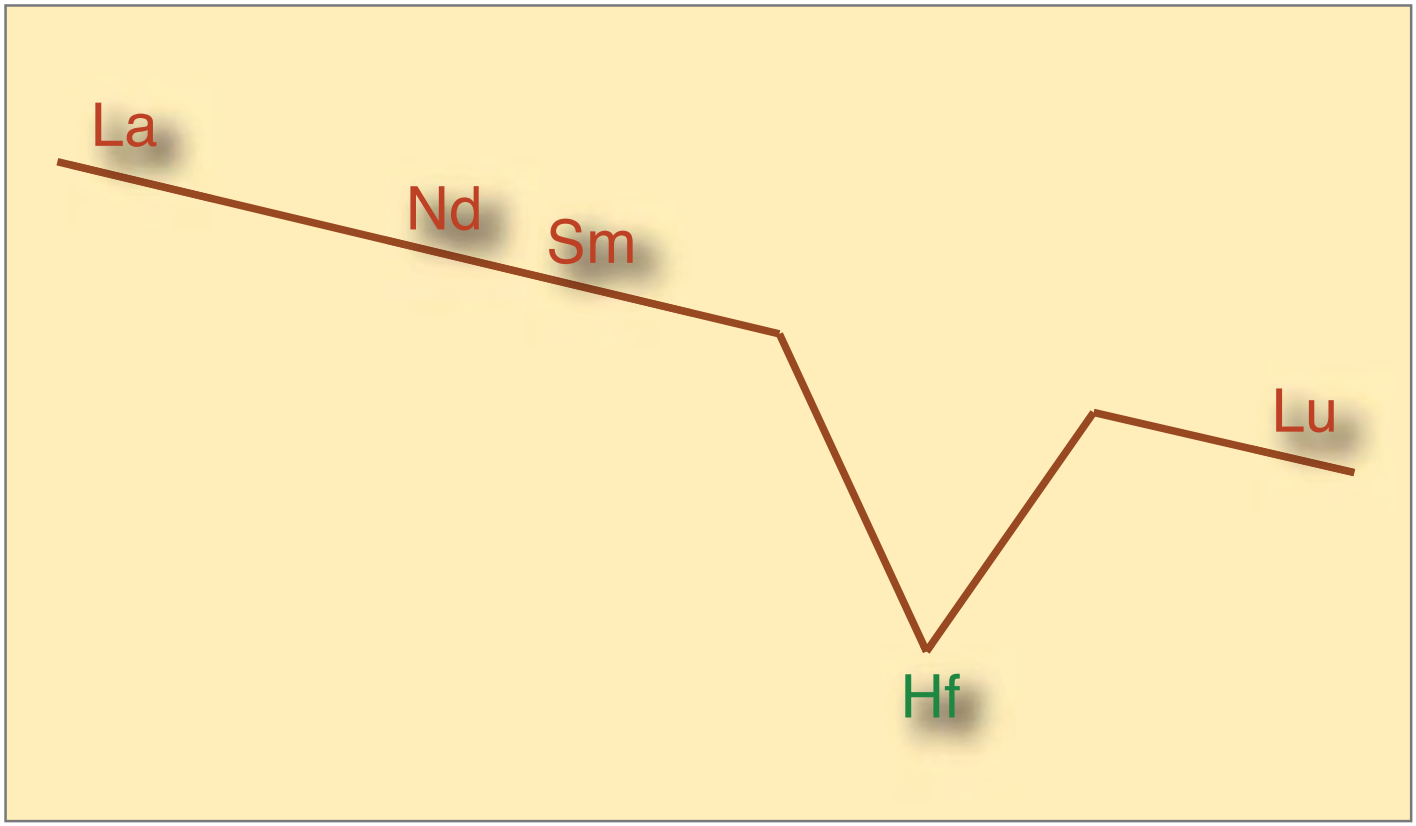

Fig. 10

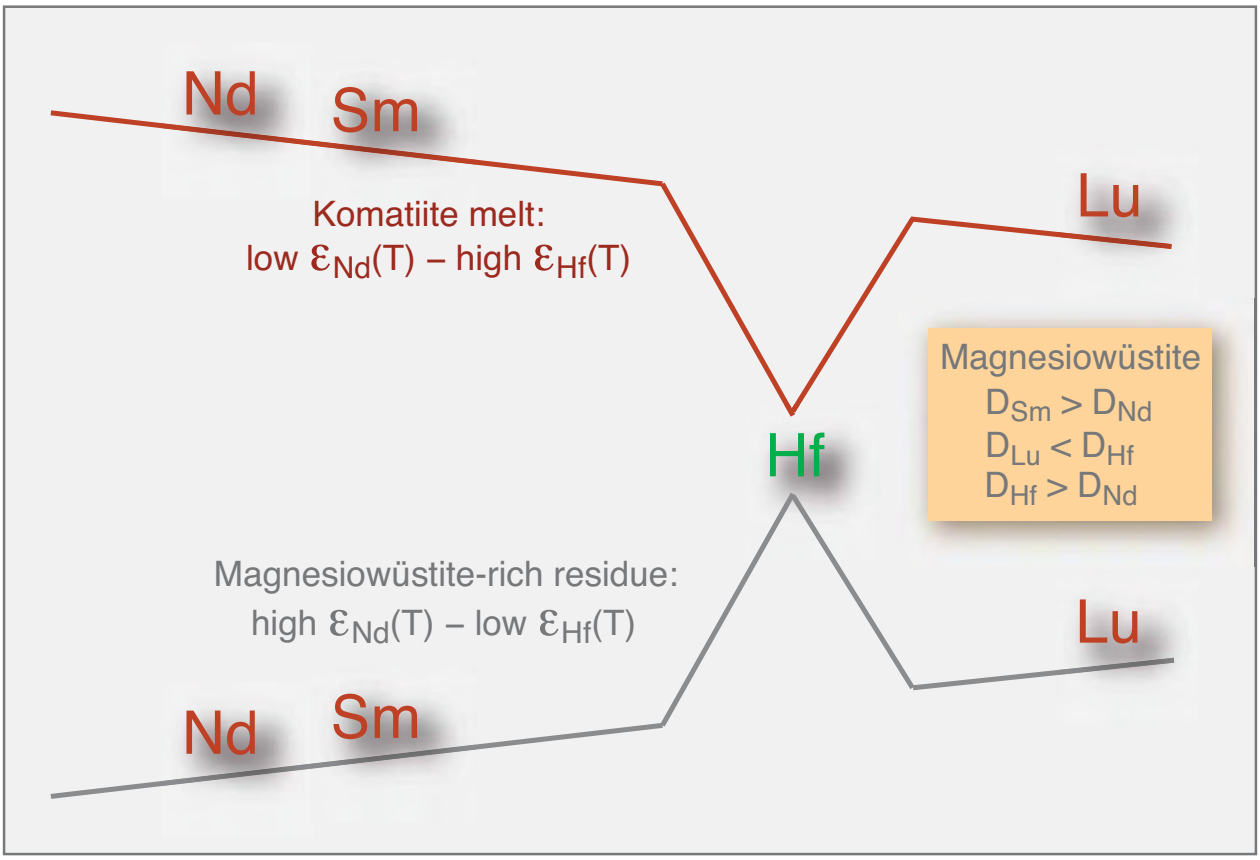
Nd
Sm
Komatiite melt:
low $\varepsilon_{Nd}(T)$ – high $\varepsilon_{Hf}(T)$
Lu
Magnesiowüstite
$D_{Sm} > D_{Nd}$
$D_{Lu} < D_{Hf}$
$D_{Hf} > D_{Nd}$
Hf
Magnesiowüstite-rich residue:
high $\varepsilon_{Nd}(T)$ – low $\varepsilon_{Hf}(T)$
Lu
Nd
Sm

Fig. 11

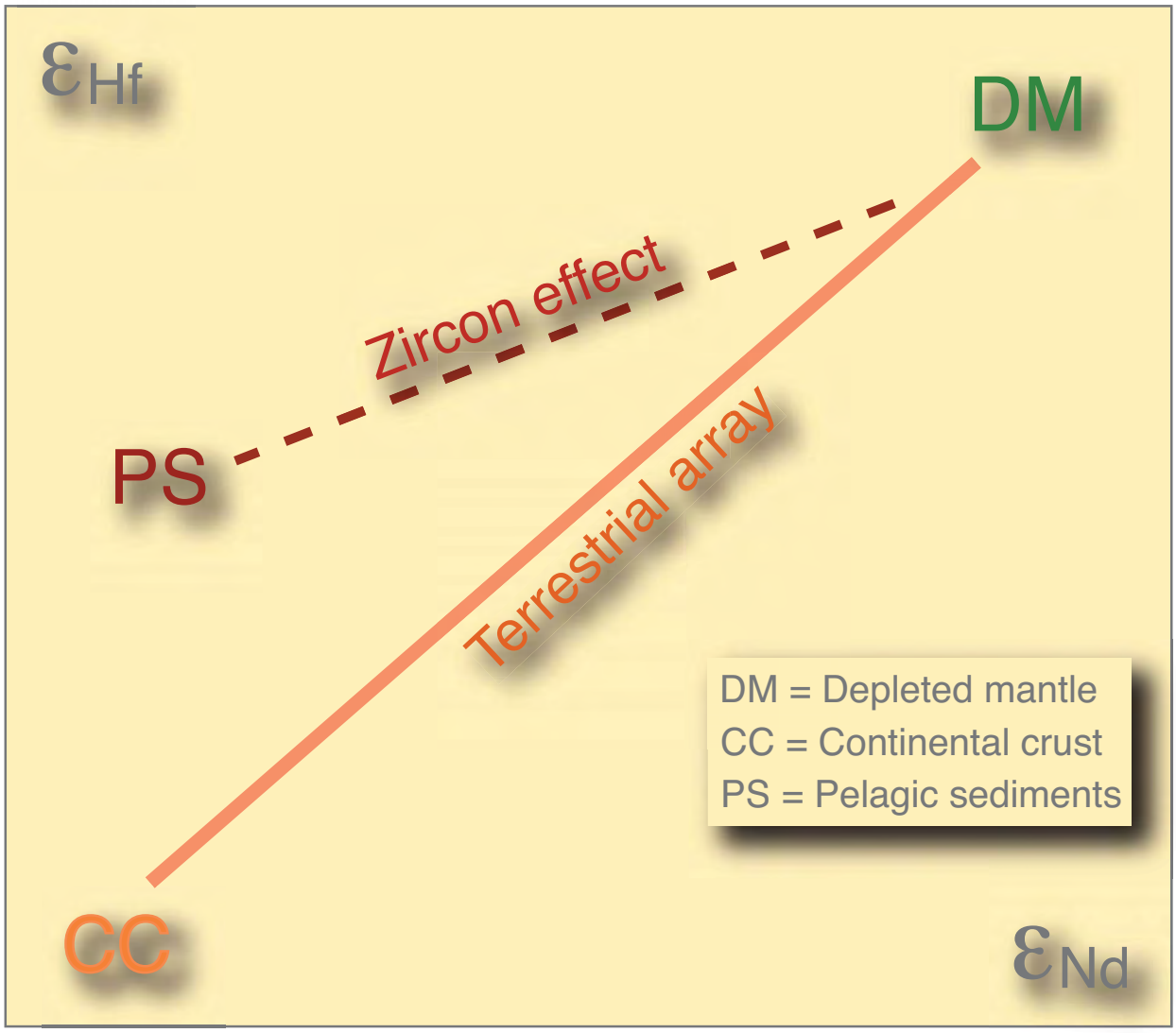
εHf
DM
Zircon effect
PS
Terrestrial array
DM = Depleted mantle
CC = Continental crust
PS = Pelagic sediments
CC
εNd

Fig. 12

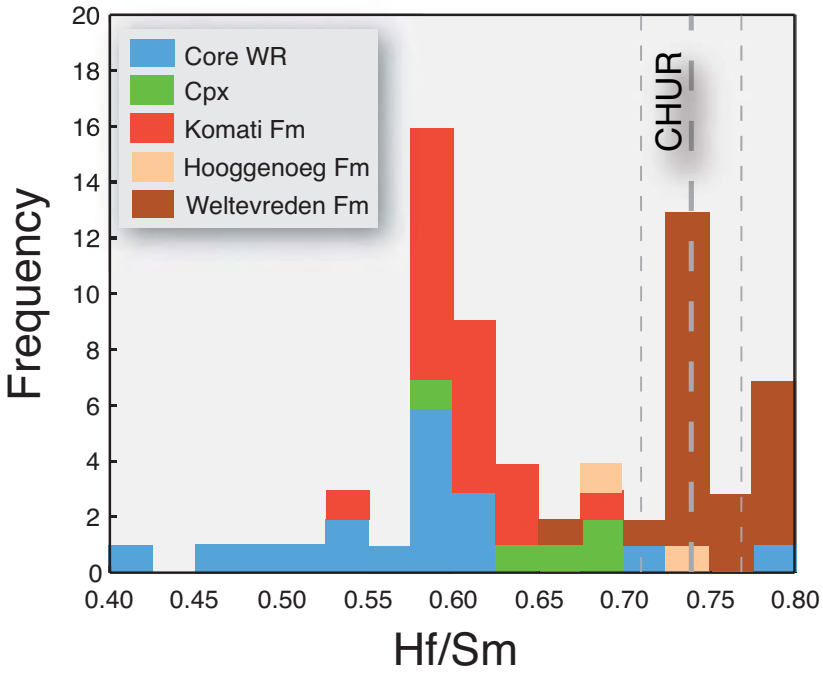
Core WR
Cpx
Komati Fm
Hooggenoeg Fm
Weltevreden Fm
CHUR
Frequency
Hf/Sm
0
2
4
6
8
10
12
14
16
18
20
0.40
0.45
0.50
0.55
0.60
0.65
0.70
0.75
0.80

Fig. 13